X-615-68-73

PREPRINT

NASA TM X- 63129

DESIGN AND CALIBRATION OF LOW FREQUENCY RADIO ASTRONOMY SPACE PROBES

RICHARD R. WEBER

FEBRUARY 1968

GSFC

GODDARD SPACE FLIGHT CENTER

GREENBELT, MARYLAND

DESIGN AND CALIBRATION OF LOW FREQUENCY RADIO ASTRONOMY SPACE PROBES

by

Richard R. Weber
Laboratory for Space Sciences
NASA-Goddard Space Flight Center
Greenbelt, Maryland

ABSTRACT

A study is made of the criteria to be used in designing a low frequency space probe. An optimizing procedure is detailed. Frequencies to be observed are set by the magnetoionic parameters $X = (\omega_p/\omega)^2$ and $Y = \omega_h/\omega$ encountered in the flight. Dipole antennas are discussed and it is shown that longer dipoles are generally desirable. Receiver types are described. Receiver input impedance is discussed. It is shown that high impedance receivers are preferable unless sensitivity is a serious problem. It is shown that a moderate imbalance in a balanced high impedance receiver can be neglected.

A calibration method is outlined. Dummy antennas are used to represent the flight antenna. The dummy antenna parameters are discussed. Receiver impedance measurements are discussed. Line lengths of less than $\lambda/1000$ are shown to be important.

Analysis of flight data is discussed. The equation relating antenna temperature to dummy antenna temperature is given.

The payload of the Astrobee 16.03 sounding rocket is

described. Launch day operations are also discussed.

Synchrotron radiation and radiative transfer are reviewed. A model spectrum is fitted to the observational data, assuming an average emission measure of 5 $cm^{-6}pc$ for the galactic radiation and 2.5 cm^{-6} pc for the extragalactic radiation.

TABLE OF CONTENTS

INTRODUCTION

The science of astronomy depended on the optical window of the earth's atmosphere for millenia as the sole channel of astronomical data. The radio window, studied for the past thirty years, is providing a vast store of new information about the universe. The radio window extends from about 10000 MHz to 10 MHz. At lower frequencies the ionosphere absorbs and reflects the incoming radio waves, preventing accurate observations. Consequently, rocket and satellite experiments above the ionosphere are necessary to carry out reliable radio astronomical measurements much below 10 MHz.

Ground based observations have shown that the intensity of the cosmic radio noise background increases toward lower frequency as $I \propto \nu^{-0.6}$ down to 10 MHz. Going below this frequency ground based measurements become increasingly uncertain, but from available space probe data and physical considerations, it is believed that the maximum intensity is reached at 2-3 MHz. Below this frequency the intensity is lower because of increased absorption by ionized hydrogen. In addition the exponent of ν for the synchrotron emission mechanism, which produces the noise, begins to increase and it becomes positive somewhere below 1 MHz. More observations are needed to clarify the nature of the spectrum between 3 MHz and the next low-frequency observing limit of about 50 kHz imposed by the interplanetary medium. Nondirectional observations will yield information on the average features of the galactic ionized

gas. Directional observations will also permit study of spectra of those sources with radiation that is not seriously affected by the intervening HII, as well as the detailed distribution of HII.

This paper describes the procedures in designing and calibrating a low frequency radio astronomy space probe. Consideration will be given to choice of receiver, antenna and antenna impedance probe, and to essential steps of calibration. Data reduction is discussed, as well as the astrophysical significance of the data. The Astrobee 16.03 payload is presented as an example of the procedures outlined.

SECTION I

SYSTEM OPTIMIZATION

A. Frequency Selection

A fundamental decision to be made in designing a system will be the choice of observing frequencies. Criteria may vary with each mission but the consideration which should always be taken is the lowest frequency to be used. For most experiments this will be set by the plasma frequency and electron gyro frequency surrounding the spacecraft. In general, higher altitudes will permit observation at lower frequencies. For a plasma radian frequency ω_p, a gyro radian frequency ω_h and an observing radian frequency ω, the magneto-ionic parameters X and Y are defined by

$$X = \left(\frac{\omega_p}{\omega} \right)^2, \quad Y = \frac{\omega_h}{\omega}$$

A plot of Y^2 vs X at several frequencies along a planned vehicle trajectory shows which frequencies will allow useful cosmic radio noise observations. See figure 1.

The origin on the X-Y^2 diagram represents the absence of plasma and magnetic fields. Region I is the only area where reliable measurements can be made at present. The notations O or E in the figure indicate propagation of the ordinary or extraordinary wave in each region. The angle between the direction of propagation and the magnetic field is Ψ.

The radiation to be observed can be considered to come from the origin (free space) and to proceed toward the point on the diagram where the radio probe is operating. At Y = 1-X the extraordinary waves will be reflected and not received if the probe is operating outside region I. The ordinary wave will be reflected at X = 1. Consequently, in regions IV, V, VII and VIII there will be essentially no cosmic radiation arriving. The ordinary wave will reach regions II, III and VI but interpretation of antenna impedance measurements is still inadequate to obtain accurate measurements from these regions.

B. Antenna Choice

A directional or nondirectional antenna may be chosen, according to the purpose of the observations and complexity of the spacecraft. Discussion of directional antennas will not be undertaken here because of the many special problems associated with each type. Dipoles will be considered in more detail.

For dipole antenna experiments it is well to recall that the antenna length does not affect the power available to a matched receiver. Any antenna can deliver a power $P_L = \frac{1}{2} SA\Delta\nu$ to a receiver, where S is the flux density, $\Delta\nu$ is bandwidth, the collecting area $A = G\lambda^2/4\pi$ and G is the gain of the antenna. If we assume the dipole pattern to be isotropic, or if we assume a uniform sky brightness distribution, we can set G = 1 and then $A = \lambda^2/4\pi$ independent of the antenna

length. However, this idealized treatment of available power falls down somewhat in real cases where shunt capacitance between the antenna extending mechanism and the spacecraft, for example, may make it difficult to match to the antenna. It also disregards ohmic loss in the antenna.

The power P_L reaching a receiver from an antenna can be determined from the equivalent circuit in figure 2. For a voltage V across the receiver resistance R_L the power is $P_L = \frac{V\ V^*}{R_L}$. By voltage division it is seen that

$$V = \frac{R_L}{(R_L+R_A)+j(X_L+X_A)}\ e$$

so that

$$P_L = \frac{e^2 R_L}{(R_L+R_A)^2+(X_L+X_A)^2}$$

Nyquist's formula relates antenna voltage e with antenna temperature T_A:

$$\overline{e^2} = 4k\ T_A\ R_A\ \Delta\nu$$

where k is Boltzmann's constant.

Thus

$$P_L = \frac{4k\ T_A\ R_A\ \Delta\nu\ R_L}{(R_L+R_A)^2+(X_L+X_A)^2} \qquad \text{Equation 1}$$

In optimizing both dipole length and receiver impedance, sufficient sensitivity and maximum measurement accuracy must be considered. The latter is best achieved by minimizing the change in received power P_L caused by a change in antenna reactance X_A, or equivalently by an error in measured receiver

reactance X_L. If received power is plotted as a function of X_A, the slope $\partial P_L/\partial X_A$ should be minimized near the expected value of X_A. A similar treatment for antenna resistance, R_A, is of less value. A change of antenna resistance may affect both the power transfer function and the available voltage if the resistance change is partially due to changed radiation resistance. In any case varying X_A will indicate about the same optimum conditions obtained by varying R_A.

Dipole antenna impedance is shown in figure 3. The parameter ℓ/λ is the half length of the antenna in wavelengths. Thus $\ell/\lambda = .25$ for a half wave dipole.

The choice of dipole antenna length is of some importance for a matched receiver as is seen in figure 4. The 0 indicates the nominal value of X_A, in this case at the peak. The power received from a short dipole will be very sensitive to small errors in reactance. In a longer dipole the sensitivity to reactance errors is decreased owing to the greater radiation resistance of the longer dipole.

Antenna length is a major factor when using high impedance receivers. Since the voltage generated in an antenna is proportional to the radiation resistance of the antenna, the system sensitivity will depend on that resistance which in turn depends on antenna length. In figure 5, increasing the antenna length sevenfold raises the sensitivity more than 20 db. An additional advantage of the longer antenna is that its radiation resistance can be determined more accurately

than when the antenna is short. The resistance of a short dipole is more difficult to determine because of the separation of the antenna driving points[1] and possible plasma sheath effects near the vehicle[2].

When contemplating the use of long dipoles one must remember that on spinning bodies with energy dissipating elements there is a strong tendency to spin around the axis having the maximum moment of inertia. Extending one long dipole from a spinning vehicle may cause a dynamic instability which leads to a shift in spin axis and catastrophic results. For this reason two dipoles are chosen when the length desired is much greater than 50 feet.

C. Receiver

The choice of receiver involves two factors: its input impedance and its type of operation. Power matching to the antenna is usually unnecessary and indeed undesirable. The error due to a small change in antenna characteristics in figure 4 is quite large compared with that for the 30000Ω curve in figure 6c. High impedance receivers minimize this error and also permit several receivers to operate simultaneously on one antenna.

The receiver is considered to begin at the driving point of the antenna and to include the shunt capacitance of the antenna extender and the cables to the receiver box. A very high impedance receiver is difficult to achieve because this shunt capacitance can drastically lower the high

impedance of the receiver. The shunt capacitance should be held to an absolute minimum by careful design of the antenna extender and by short cable runs or unshielded cables. Separate preamplifiers near the antennas can help in shortening cable runs. Figure 7 shows the effect of different shunt capacitances on the slope $\partial P_L/\partial X_A$. Receivers are treated as parallel circuits in these figures because this is a good physical description of their characteristics.

Given the minimum practical receiver shunt capacitance, the optimum shunt resistance must be found to minimize $\partial P_L/\partial X_A$ near the operating point. This value of shunt resistance is not the highest possible resistance, as is frequently assumed, but depends on frequency and shunt capacitance. See the examples in figure 6. At a given frequency the optimum shunt resistance is equal to the magnitude of the shunt reactance. This provides the maximum series resistance and reduces the sensitivity of P_L in equation 1 to changes in reactance. A compromise must then be found for the frequency range to be observed.

The frequency response of the front end of the receiver must have a steep roll-off well below the ionospheric critical frequency or it may be affected by RF break-through from the ground. This RF break-through could saturate the receiver and render the calibration useless.

There is a variety of receiver types which can be used. Each of them has certain strong and weak points. Among the

advantages to be weighed for a particular mission are fast response, long-term stability, continuous coverage of each frequency, multi-frequency capability, dynamic range and intensity resolution. A related decision will involve telemetry capability and desired time resolution. A tuned radio-frequency receiver, for example, will give fast response and good time resolution. Its penalties are single frequency operation and full time need for one or more telemetry channels. The Ryle-Vonberg configuration provides good long term stability and several frequencies in sequence. Its shortcomings are slow response and complexity. Several types of swept frequency receivers offer advantages of wide spectral coverage in either continuous or closely stepped increments of frequency. Unless the receiver can be swept rapidly, it will not provide good coverage at any single frequency. Additionally, swept receivers are more tedious to calibrate adequately.

A receiver audio channel available for pre-flight evaluation of the spacecraft Radio Frequency Interference (RFI) problems is a very valuable asset. One of the major problems in low frequency cosmic radio noise experiments to date has been RFI generated on the payload.

A flight noise source should be included in any payload as a means of checking the receivers. This is very convenient during ground checks and is essential during flight for any type receiver.

D. Effects of Inequalities in Balanced Systems

To determine the effect of inequalities of the impedances on two sides of a balanced system, consider one-half of the dipole and one preamplifier in figure 8. If the half dipole impedance is $Z_A/2$, half dipole voltage $e_A/2$, preamp impedance $Z_L/2$, and the preamp voltage gain g, the output voltage of a preamp is

$$V_i = g \frac{Z_L/2}{Z_L/2+Z_A/2} \frac{e_A}{2} = g \frac{Z_L}{Z_L+Z_A} \frac{e_A}{2}$$

Let us define a complex ratio r by $Z_L = r\, Z_A$. Then

$$V_i = g \frac{r\, Z_A}{(r+1)Z_A} \frac{e_A}{2}$$

$$V_i = g \frac{r}{r+1} \frac{e_A}{2} \qquad \text{Equation 2}$$

For a high impedance receiver, $|r| >> 1$, and small differences between the r for each half of the system are negligible. Thus if the two preamps have slightly different impedances, it has almost no effect.

If r is on the order of 1 the two sides must be more nearly the same. For the two voltages V_i to be within 5% for example, if we assume the antenna halves produce equal voltages and the gains are equal, it is required that r_1/r_1+1 be within 5% of r_2/r_2+1. If $r_1 = 2$, then the requirement is

$$1.73 < r_2 < 2.33$$

This wide range indicates that unequal preamplifier impedances should not present much difficulty.

If the gains of the two preamplifiers are unequal this produces an imbalance proportional to the inequality, regardless of the input impedance of the preamps. Therefore, care should be taken to make the gains equal.

It might be thought that any inequalities are calibrated out and do not matter. This is only true if each side is calibrated essentially separately accounting also for any inequalities in the two halves of the dummy antenna which is used in calibration.

If the preamp output voltage V_i is phase shifted by an amount $\Delta\phi_i$, the difference between the shifts in the two preamps, $\Delta\phi = \Delta\phi_1 - \Delta\phi_2$, should be near zero. As $\Delta\phi$ departs from zero the voltage V_R drops. This decreases the sensitivity as cos $\Delta\phi$. More importantly, an error caused by a drift of $\Delta\phi$ after calibration will increase as $\sin\Delta\phi$, so an initial $\Delta\phi = 0$ provides the maximum accuracy. Therefore the two phase shifts $\Delta\phi_1$ and $\Delta\phi_2$ should be made as equal as possible across the range of observing frequencies.

E. Flight Impedance Measurements

An impedance probe, Z-meter or capacitance probe is required for any experiment which may at times operate outside of region I of the $X\text{-}Y^2$ diagram. Without it, one cannot be sure where each frequency is operating on this diagram. The probe will be switched periodically on to the antenna to determine antenna impedance or at least its capacitance.

SECTION II

CALIBRATION PROCEDURES

A. Equipment Preparation

1. Noise source

A radio-frequency noise source is the preferred means of receiver calibration. Using a monochromatic signal would require accurate knowledge of the bandpass and detector characteristics of the receiver. The noise source should have a spectrum shaped like that of the expected cosmic noise background. This will produce harmonics and intermodulation in the receiver front end in a similar degree for calibration as occurs during flight so that these problems can be neglected. The necessary noise temperatures are on the order of 10^{14}°K. These temperatures are required to calibrate for expected sky brightness temperatures near 10^{7}°K while allowing for perhaps an additional 30 db dynamic range above 10^{7}°K in the receivers and allowing for up to 40 db loss in the dummy antennas used in calibration. Figure 9 shows one scheme for determining the output temperature of the noise source.

The Wayne Kerr SR268 receiver used with a time constant of .25 sec was adequate to detect .1 db changes of the attenuator setting, allowing .05 db or 1% accuracy. This is sufficient because the standard noise sources available are accurate to no better than 1%.

Frequent checks on noise output during calibration

are desirable. In routine checks a broadband RF voltmeter should be adequate to show any shift in noise output. It is advisable to repeat the detailed noise source calibration after payload calibration and prior to launch.

2. Dummy antennas

A dummy antenna allows a known amount of noise power from a calibrated noise source to be put into the receiving system from a source of the same impedance as the antenna. Although the receiver could, in principle, be calibrated from a 50 ohm source, the corrections for flight antenna impedance would be much larger and consequently more prone to error. Also the noise figure of the receiver may vary with the impedance it sees, so using a dummy antenna impedance similar to the flight antenna will minimize this effect. Figure 10 shows a dummy antenna. The transformer secondary impedance R_S is 10 or 20 times the antenna resistance R_A. Thus, the output impedance of the dummy antenna box is approximately R_A in series with C_A. The cables of electrical length l_e which attach to the box are included in the dummy antenna. These cables may be chosen to represent the capacitance of the antenna extension mechanism if it is not electrically included in the calibration. Otherwise, they should be as short as possible.

When measuring the impedance of the dummy antenna, cables of the same electrical length l_e are used to attach to the impedance bridge. Thus, the effect of the cable need not

be calculated and removed from the measurement. A simple means of determining electrical length is shown in figure 11. The voltmeter reads a minimum when the open line is a quarter wavelength. By finding the lowest frequency for a minimum voltage when both cables are attached f_B, and for when only the test cable is attached f_T, one can determine the electrical length of the unknown cable from

$$l_e = \frac{300}{4f_T} - \frac{300}{4f_B}$$

where f_B and f_T are in MHz and l_e is in meters.

The dummy antenna temperature T_{DA} can be determined at a given frequency using a narrow band signal at that frequency. See figure 12. By measuring the loaded generator voltage e_i and the open circuit output voltage e_o one has:

$$e_g^2 = 4k\ T_g\ R_g\ \Delta\nu$$

$e_i^2 = k\ T_g\ R_g\ \Delta\nu$ since $e_i = \frac{1}{2}\ e_g$ for DA input impedance of 50Ω

$$e_o^2 = 4k\ T_{DA} R_o\ \Delta\nu = \left(\frac{e_o}{e_i}\right)^2\ e_i^2$$

Now $\left(\frac{e_o}{e_i}\right)^2$ can be determined using an RF voltmeter.

Thus

$$T_{DA} = \frac{\left(\frac{e_o}{e_i}\right)^2\ e_i^2}{4k\ R_o\ \Delta\nu} = \frac{\left(\frac{e_o}{e_i}\right)^2\ k\ T_g\ R_g\ \Delta\nu}{4k\ R_o\ \Delta\nu}$$

$$T_{DA} = \left(\frac{e_o}{e_i}\right)^2 \frac{T_g R_g}{4\ R_o} \qquad \text{Equation 3}$$

This equation will then hold for a noise generator with the receiver defining the operating frequency.

3. Impedance probe loads

The impedance probe should be calibrated over a wide range if magnetoionic resonances will be encountered. These may change the antenna impedance by more than an order of magnitude[3,4]. Either series or parallel loads can be used. The loads must be measured at RF to determine their exact value.

B. Receiver Impedance Measurements in Payload

The receiver is considered to include the cables and relays which connect to the antennas. It also includes the capacitance of the antenna extender. The measurements of receiver impedance are taken either at the cables attaching to the antenna or if possible through a second connector on the antenna. The unbalanced and balanced impedances are measured at each frequency. The cables connecting the bridge to the receiver should be measured for electrical length and their effect removed via the equation:

$$Z_{RCVR} = Z_o \frac{Z_{BR} - jZ_o \tan\theta}{Z_o - jZ_{BR} \tan\theta} \qquad \text{Equation 4}$$

$$\theta = \frac{2\pi\, l_e}{\lambda}$$

Z_{BR} = impedance bridge reading

Z_{RCVR} = receiver impedance

Z_o = cable characteristic impedance

It should be pointed out that in high impedance systems line lengths of even less than $\lambda/1000$ cannot be neglected if accurate calibration is to be achieved. A simple rule of thumb at these frequencies is to account for all lines larger than 1 centimeter. For example with a bridge reading of Z_{BR}=5000-j5000 at $\lambda/1000$ from the receiver, using a balanced pair of 50Ω cables (effectively 100Ω) the receiver impedance is found using equation 4 to be Z_{RCVR} = 8785-j3267. If the cables had simply been represented as a lumped capacitance the receiver impedance would have been calculated to be Z_{RCVR}=9945+j740. Thus it is clear that the line lengths must be treated properly.

C. Receiver Noise Calibration in Payload

The receiver is calibrated using the high level noise source and the dummy antennas as in figure 13. The attenuator is stepped through the dynamic range of the receiver. This procedure is repeated at several receiver temperatures. Figure 14 shows the dynamic response of a Ryle Vonberg receiver calibrated using an automatic system which steps the attenuator and puts the receiver output voltages directly on punched cards for computer plotting. Such a system is nearly indispensable for calibration of many frequencies at several temperatures.

These Ryle Vonberg receivers have three 20 db ranges for a total dynamic range of 60 db. The fine and coarse outputs provide redundant information. The repeatability of the data at each temperature is generally better than .1 db.

D. Impedance Probe Calibration

Figure 15 shows an impedance probe. The signal oscillator excites the antenna. The current channel on the right picks up a signal proportional to the current amplitude. The voltage channel on the left measures the voltage applied to the antenna. These two channels are combined to produce a phase channel. The magnitude and phase of the impedance are then determined by V/I and the phase between V and I.

The probe must be calibrated over a wide range if magnetoionic impedance resonances will be encountered. These resonances occur at X=1 and $Y^2=1-X$[3,4]. Observing them at several frequencies and different altitudes can be used as a means of determining and electron density profile. This will indicate where on the X-Y^2 diagram the payload is operating at each frequency and which frequencies are supplying reliable data.

The simplest means of calibrating the impedance probe satisfactorily is to calibrate at the ends of cables having the same electrical properties, length and discontinuities, as the payload cables leading from the antenna to the impedance probe. If the actual payload cables can be used, this is preferable. This may be impossible because the separation of the cables will not allow the attaching of a calibration load across the two cables. Calibration directly at the probe will require transformation from the probe to the end of the payload cables using equation 4 where Z_{RCVR} becomes the desired

antenna impedance and Z_{BR} is the impedance seen by the probe. The probe calibration is done at several temperatures.

A useful check is to attach the dummy antennas on the impedance probe cables and see if the probe calibration curves give the correct value for the dummy antenna impedance.

E. Temperature Sensor Calibration

Temperature sensors are strategically mounted in each enclosure containing active components in the payload. The output voltage of each temperature sensor is monitored when the receiver and impedance probe calibration is in progress.

F. Antenna Base Impedance

Measurement of the unbalanced and balanced impedance of the antenna extenders at each frequency is necessary to permit calculation of the receiver impedance if this base impedance is not included in the receiver impedance measurements.

The capacitance between the antenna and the spacecraft may be included in the base impedance. It is obtained by measuring the impedance of a monopole in a half model of the spacecraft over a ground plane. It is generally small and in some cases negligible.

SECTION III

ANALYSIS OF FLIGHT DATA

A. Antenna Impedance

The measured impedance is found from the impedance probe calibration curves for the appropriate measurement frequency and probe temperature. Corrections are made if necessary for cable lengths and antenna base capacitance.

B. Radiation Efficiency

Antenna radiation efficiency is defined in the transmitting sense as

$$\eta_R = \frac{\text{Power radiated}}{\text{Power input}} = \frac{i^2 R_A}{i^2 R_A + i^2 R_\Omega} = \frac{R_A}{R_A + R_\Omega}$$

where R_A is the radiation resistance and R_Ω is the ohmic resistance of the antenna. For a short dipole decreasing the frequency will lower R_A more rapidly than R_Ω. Also R_Ω will reach a terminal value when the skin depth which would carry the current exceeds the available thickness of the antenna tubing. Thus η_R decreases toward lower frequency.

In a power matched system η_R must be accounted for carefully. Fortunately however, with a high impedance receiver η_R can be neglected even though it may be small. Consider the simplified receiving circuit in figure 16. The fundamental quantity to be measured is the power P_L delivered to the receiver

$$P_L = \frac{V^2}{R_L} = \frac{e^2 R_L}{(R_L + R_A + R_\Omega)^2}$$

If $R_L >> R_\Omega$ the value of R_Ω is unimportant to P_L although it may be that $R_\Omega \geq R_A$ and $\eta \leq 0.5$. For example if $R_L \geq 200 \cdot R_\Omega$ and $\eta = 0.1$ the error involved in assuming $\eta = 1$ is less than 1%.

C. Antenna Temperature

The receiver input power is determined from the receiver calibration curves. The antenna impedance found above and this measured power are used to determine the antenna temperature with the equation

$$T_A = \frac{(R_L'+R_A)^2+(X_L'+X_A)^2}{(R_L+R_{DA})^2+(X_L+X_{DA})^2} \frac{R_{DA}R_L}{R_A R_L'} T_{DA} \qquad \text{Equation 5}$$

where T_A = antenna temperature

T_{DA} = dummy antenna temperature for same receiver response

R_A+jX_A = antenna impedance

$R_{DA}+jX_{DA}$ = dummy antenna impedance

R_L+jX_L = load impedance seen by dummy antenna

$R_L'+jX_L'$ = load impedance seen by flight antenna; this differs from R_L+jX_L by capacitance of antenna to payload and by antenna mechanism capacitance if it is not included in R_L+jX_L.

This equation is derived from equation 1 by equating calibration and flight powers P_L. It is valid if R_L differs from R_L only by non-dissipative capacitance.

SECTION IV

DESCRIPTION OF ASTROBEE 16.03 PAYLOAD

A. System Description

The Astrobee 16.03 payload consisted of two receivers, two orthogonal 120 foot dipoles, an impedance probe, a voltage regulator, a programmer, temperature sensors, three orthogonal magnetometers and other ancillary equipment.

The Ryle-Vonberg receivers were designed by C. R. Somerlock for the RAE satellite program. They each contained eight frequency channels operating sequentially. The frequency range was 600 KHz to 3.93 MHz. Useful cosmic noise data were anticipated down to 800 KHz, with the possibility of data at lower frequencies if the rocket went higher than predicted or if the electron density profile was lower than expected. The Ryle Vonberg receiver is not the best type for a sounding rocket because of its slow response and complexity and because its long term stability is unneeded. Its use on this flight was intended to provide a flight check of the receivers before launch of RAE.

A block diagram of the Ryle Vonberg receiver is seen in figure 17. The antenna noise is compared with a calibrated internal noise source. The output of the noise source is adjusted by a servo loop to equal the unknown antenna noise. A measurement of the internal noise source by a thermistor bridge provides the fine output. The coarse output is the

servo loop feedback voltage. The noise source has a 20 db range. Together with the attenuator which has three ranges, the receiver covers a 60 db dynamic range.

The 120 foot dipoles chosen were the longest available antennas in an acceptable package size. Two dipoles were used to insure spin stability and to provide redundancy. One receiver operated on each dipole and the two systems were electrically independent. Each boom had a microswitch which registered every 1.4 inches of deployment as the antennas extended.

The impedance probe operated at five frequencies: 0.7, 0.8, 0.9, 1.0 and 2.8 MHz. It was switched on each dipole for 1.5 seconds every 12 seconds. The greatest value of the probe is to show when the resonances $X=1$ and $Y^2=1-X$ are encountered at each frequency. From this information it is possible to determine where each frequency is operating on the $X-Y^2$ diagram.

B. Block Diagram and Photograph of Payload

The 16.03 experiment configuration is shown in figure 18. Each antenna was connected via relays to either a receiver or the impedance probe. When the probe was on an antenna, the receiver input was shorted. The probe was also periodically switched to calibration loads at each antenna.

Figure 19 shows the payload. Visible are an antenna mechanism and the cylindrical impedance probe with preamplifiers for receiver 1 beside it. Part of receiver 1 and 2 and the

programmer can be seen on the next deck. The top two decks contain batteries, telemetry and magnetometers.

C. Vehicle Description

The Astrobee is a developmental two-stage rocket weighing over $5\frac{1}{2}$ tons. It can carry a 100 pound payload to an altitude of 2300 kilometers on a 30 minute flight. The vibration levels reach 12g and acceleration reaches 41g. Figure 20 shows the vehicle on launch day.

D. Launch Day Operations

On launch day the chief scientific requirements for launch were a quiet sun, a sufficiently high ionospheric critical frequency, a shutoff of the Alouette satellite sounder and a properly functioning experimental payload and launch vehicle.

Monitoring of two 30 MHz riometers at separate locations was conducted at Wallops Station. Quiet conditions in the ionosphere as well as on the sun were indicated for several hours preceding the flight. Real time data from solar, optical and radio observatories, collected at the Environmental Sciences Service Administration Center in Boulder, Colorado, were examined continuously up to the time of launch. Information from the University of Colorado solar radio spectrograph was most important in the attempt to avoid low frequency solar bursts.

The Wallops Station ionosonde provided repeated ionospheric soundings until just before launch and it resumed again after the flight.

The Alouette II Sounding Satellite was within range of the rocket trajectory and was turned off for the rocket flight by ground command.

The payload operated well during ground checks on launch day.

E. Flight

At 135 seconds after launch yoyos were scheduled to despin the vehicle from 4 rps to .08 rps to permit the experiment antennas to deploy safely. The despin mechanism failed completely. At 145 seconds after launch all four antenna booms came out on schedule. When they had extended six feet the deployment rate of two suddenly increased due to the large centrifugal forces. They then bent from the Coriolis force and wrapped around the vehicle. The impedance probe showed that the antennas were shorted. The extension mechanisms jammed with only about 9 feet of tape deployed. The spin rate dropped from 4 rps to 3 rps as a result of the partial deployment. The receivers both remained at the bottom of their dynamic range throughout the remainder of the flight. No astronomical information was obtained.

The payload reached an altitude of 2300 km and impacted at $39^{\circ}.93$ north latitude and $56^{\circ}.38$ west longitude, 1200 km from the predicted point.

SECTION V

INTERPRETATION OF LOW FREQUENCY COSMIC RADIO NOISE

A. Synchrotron Radiation

An low energy electron or positron in a magnetic field will spiral around the lines of force in a helical path. The frequency of the motion is the gyro frequency

$$\nu_h^o = \frac{\omega_h^o}{2\pi} = \frac{e\,H}{2\pi\,mc}$$

where H is the magnetic field component normal to the velocity of the particle. The electron will radiate as a dipole at this frequency. If an observer is situated in the orbital plane of the electron most of the apparent acceleration of the electron occurs as it approaches or recedes from the observer. If the electron is relativistic (v near c) the radiation field is enhanced as the electron approaches because the electron is moving in the direction of the field. When the electron recedes the radiation field is attenuated. The resulting observed radiation is concentrated along the velocity vector in a cone of dimension

$$\theta = \frac{mc^2}{E} = \frac{5\text{x}10^5\text{ev}}{E}$$

where E is the total energy of the electron.

The radiation is received as a series of pulses of short duration which occur when the electron is approaching the observer. If the electron is relativistic its gyro frequency becomes

$$\nu_h = \frac{\omega_h}{2\pi} = \frac{e\ H}{2\pi\ mc} \sqrt{1 - \frac{v^2}{c^2}} = \frac{e\ H}{2\pi\ mc} \left(\frac{mc^2}{E}\right)$$

The pulses from the electron are very short and continue for some finite time. Fourier analysis shows that the electron radiates at its fundamental frequency ν_H and harmonics each with finite bandwidths. The resultant is an essentially continuous spectrum.

The frequency where this continuous spectrum has its maximum intensity is given by

$$\nu_{max} = \frac{\omega_{max}}{2\pi} = \frac{e\ H}{2\pi\ mc} \left(\frac{E}{mc^2}\right)^2 \simeq 4.6 \times 10^{12} H\ (E_{BeV})^2$$

Thus it is evident that higher energy electrons will radiate at higher frequency. The critical or average frequency radiated by the electron is

$$\nu_c = \nu_{max}/.29$$

Figure 21 shows the cosmic ray electron spectrum. It can be seen that low energy electrons are much more numerous than high energy electrons. This is the reason why more cosmic radio noise is radiated at lower frequencies. The cosmic ray spectrum may be approximated by

$$N(E)\ dE = K\ E^{-\beta}\ dE \qquad \text{Equation 6}$$

The exponent $-\beta$ is the slope of the curve in the logarithmic plot. It is clear from the observations that β varies with electron energy.

The intensity of the cosmic radio noise is related to the cosmic rays by

$$I = f(e,m,\beta,K,R)\nu^{(1-\beta)/2}\ H^{(1+\beta)/2} \qquad \text{Equation 7}$$

where K and β are defined by equation 6

R is the distance from the observer.

Assuming a magnetic field of 2×10^{-6} oersted the characteristic frequency ν_c given in Equation 6 and 7 is found to be 1 MHz for .18 BeV electrons and 10 MHz for .57 BeV electrons.

Figure 22 shows the observed low frequency cosmic noise data. The spectrum turns over at 2-3 MHz if the few high points below 1 MHz are assumed to be due to some phenomenon in the solar system. The turnover is due in part to the change in slope of the cosmic ray spectrum, but it is more the result of free-free-absorption in the interstellar ionized hydrogen.

B. Radiative Transfer

Consider radiation passing through a cloud of ionized gas. The change of intensity of a beam contained in a cylinder 1 cm^2 in cross section can be written as

$$\frac{dI_\nu}{ds} = -k_\nu I_\nu + j_\nu$$

where k_ν = volume coefficient of absorption

j_ν = volume emissivity

Defining optical depth by $d\tau_\nu = k_\nu\, ds$ the equation becomes

$$\frac{dI_\nu}{d\tau_\nu} = -I_\nu + \frac{j_\nu}{k_\nu} = -I_\nu + J_\nu$$

where J_ν is called the source function. This equation is satisfied by a solution of the form

$$I_\nu = a(\tau_\nu)e^{-\tau_\nu}$$

$$\frac{dI_\nu}{d\tau_\nu} = \frac{d\ a(\tau_\nu)}{d\tau_\nu}\ e^{-\tau_\nu} - a(\tau_\nu)e^{-\tau_\nu} = -\ a(\tau_\nu)e^{-\tau_\nu} + J_\nu$$

$$\frac{d\ a(\tau_\nu)}{d\tau_\nu} = J_\nu\ e^{\tau_\nu}$$

$$a(\tau_\nu) = \int_o^{\tau_\nu} J_\nu\ e^{t_\nu}\ dt_\nu + I_o$$

Thus $$I_\nu = \int_o^{\tau_\nu} J_\nu\ e^{t_\nu - \tau_\nu}\ dt_\nu + I_o\ e^{-\tau_\nu}$$

The observed intensity I_ν consists of a contribution from the cylinder in the integral term and the original intensity I_o reduced by $e^{-\tau}$.

If the cloud being considered contains a thermal gas, e.g. HII, then

$$J_\nu = B_\nu(T) = \text{Planck's function}$$

Assuming a uniform temperature in the cloud makes $B_\nu(T)$ constant:

$$I_\nu = B_\nu(T) \int_o^\tau e^{t_\nu - \tau_\nu}\ dt + I_o e^{-\tau_\nu}$$

$$= B_\nu(T)(1-e^{-\tau}) + I_o e^{-\tau_\nu}$$

In terms of temperatures this becomes

$$T_b = T_e\ (1-e^{-\tau_\nu}) + T_n\ e^{-\tau_\nu} \qquad \text{Equation 8}$$

where T_b = observed brightness temperature

T_e = electron temperature of HII region

T_n = incident nonthermal brightness temperature

At frequencies below 10 MHz the nonthermal brightness temperature of synchrotron radiation T_n will be much greater than the thermal brightness temperature T_e of HII regions. In equation 8 $T_b = T_n$ when the cloud is absent. As the cloud opacity increases T_b decreases until for high opacity $T_b = T_e$. At 1 MHz for example, $T_n \cong 2.6\times10^7\ ^oK$ whereas $T_e \cong 12000^o$ independent of frequency. Consequently a region of HII in front of a bright nonthermal source will absorb most of the nonthermal radiation below MHz. The region will then appear as a dark area in the sky because $T_e << T_n$ at low frequency.

C. A Model Spectrum

The brightness temperature for a uniform mixture of thermal and nonthermal emitters is[5]

$$T_b = (T_e + \frac{T_n}{\tau})(1 - e^{-\tau})$$

Below 10 MHz, $T_e << T_n$ and one has

$$T_b = T_n \frac{(1-e^{-\tau})}{\tau}$$

This equation represents the galactic component of the observed

low frequency emission where it is assumed that the galactic emission originates in a mixture of thermal and nonthermal radiators.

The optical depth τ is given by

$$\tau \approx 0.5 \frac{\langle N_e^2 L \rangle}{\nu_{MHz}^2}$$

where $\langle N_e^2 L \rangle$ is the emission measure

$$\langle N_e^2 L \rangle = \int_o^s N_e N_i \, ds = \int_o^s N_e^2 \, ds$$

This emission measure gives the average of the square of the electron density along a line of sight.

The isotropic radio noise component is attenuated by the galactic ionized gas between the sun and the extremities of the galaxy

$$T_b = T_n e^{-\tau}$$

The isotropic radiation is received chiefly from the higher latitudes because $\tau \alpha \csc b$.

The galactic brightness temperature is found to vary as

$$T_b \alpha \nu^{-2.44}$$

in the range of 10-100 MHz. The isotropic brightness temperature varies as

$$T_b \alpha \nu^{-2.67}$$

in the same frequency interval. Extrapolating these spectra

to lower frequency one can determine an optical depth and emission measure for each component to fit the observational data.

At frequencies below 0.5 MHz the isotropic component is almost entirely gone due to absorption. At ~3 MHz it is reasonable to believe that the isotropic intensity exceeds the galactic. Above 10 MHz the steeper slope of the isotropic radiation causes it to fall below the galactic component again. Figure 23 shows the galactic and isotropic components and the total spectrum. The two components have been set equal at 7 MHz. Figure 22 shows the calculated total spectrum and the observational data.

A better model awaits further observations.

SELECTED BIBLIOGRAPHY

Alexander, J. K. and R. G. Stone, "Rocket Measurements of Cosmic Noise Intensities Below 5 Mc/s", Ap. J. 142, 1327, 1965.

Alexander, J. K., R. R. Weber and R. G. Stone, "Measurements of the Cosmic Radio Noise Spectrum Near the Low Frequency Turnover", Astron. J. 72, 289, 1967.

(2) Bachynski, M. P., "Sources in Plasmas", RCA Rev., 28, 111, 1967.

Benediktov, E. A., G. G. Getmantsev, Yu. A. Sazanov and A. F. Tarasov, "Results of Measurements of Radio Emission at 725 and 1525 Kc by Equipment on the Satellite Elektron 2", Kosm. Issled. 3, 614, 1965.

Bleeker, J. A. M., J. J. Burger, A. J. M. Deerenberg, A. Scheepmaker, B. N. Swanenburg and Y. Tanaka, Proc. Tenth Internat. Conf. on Cosmic Rays, 1967.

Bridle, A. H., "The Spectrum of the Radio Background Between 13 and 404 MHz", Mon. Not. R. Astr. Soc. 136, 219, 1967.

Ginzburg, V. L. and S. I. Syrovatskii, "Cosmic Magnetobremsstrahlung", Ann. Rev. Astron. and Ap. 3, 297, 1965.

Hartz, T. R., "Observations of the Galactic Radio Emission Between 1.5 and 10 MHz from the Alouette Satellite", Ann. d'Ap. 27, 823, 1964.

Huguenin, G. R. and M. D. Papagiannis, "Spaceborne Observations of Radio Noise from 0.7 to 7.0 MHz and their Dependence on the Terrestrial Environment", Ann. d'Ap. 28, 239, 1965.

Jokipii, J. R., J. L'Heureux and P. Meyer, "Diurnal Intensity Variation of Low Energy Electrons Observed near the Polar Cap", J. Geophys. R., 72, 4375, 1967.

(1) King, R. and T. W. Winternitz, "The Cylindrical Antenna with Gap", Quart. of Appl. Math. 5, 403, 1948.

Korobkov, Yu. S., "The Spectrum of Distributed Cosmic Radio Emission in the Decameter Range of Radio Waves", IVUZ Radiofizika. 7, 982, 1964.

L'Heureux, J., "The Primary Cosmic Ray Electron Spectrum Near Solar Minimum", Ap. J. 148, 399, 1967.

Oya, H., "Effect of Resonances on the Admittance of an RF Plasma Probe Surrounded by an Ion Sheath", Rep. of Ionosphere and Plasma Research in Japan, 19, 243, 1965.

Purton, C. R., "The Spectrum of the Galactic Radio Emission", Mon. Not. R. Astr. Soc. 133, 463, 1966.

Ramaty, R. and R. E. Lingenfelter, "Galactic Cosmic-Ray Electrons", J. Geophys. R. 71, 3687, 1966.

Slysh, V. I., "The Measurement of Cosmic Radio Emission at 210 and 2200 Kilocycles per Second to Eight Earth Radii on the Automatic Interplanetary Station Zond 2", Kosm. Issled. 3, 760, 1965.

Smith, F. G., "Cosmic Radio Noise as Measured in the Satellite Ariel II. Part II, Analysis of the Observed Sky Brightness", Mon. Not. R. Astr. Soc. 131, 145, 1965.

Stone, R. G., J. K. Alexander and R. R. Weber, "Magnetic Field Effects on Antenna Reactance Measurements at Frequencies well above the Plasma Frequency", Planet. Space Sci. 14, 1227, 1966.

(3) Stone, R. G., J. K. Alexander and R. R. Weber, "Measurements of Antenna Impedance in the Ionosphere II, Observing Frequency Greater than the Electron Gyro Frequency", Planet. Space Sci. 14, 1007, 1966.

Stone, R. G., R. R. Weber and J. K. Alexander, "Experimental Measurements on a Dipole Antenna in the Ionospheric Plasma", presented at Fall 1967 URSI and IEEE G-AP Meetings, Ann Arbor, Mich., 16-19 October 1967.

(4) Stone, R. G., R. R. Weber and J. K. Alexander, "Measurement of Antenna Impedance in the Ionosphere I, Observing Frequency Below the Electron Gyro Frequency", Planet. Space Sci. 14, 631, 1966.

Walsh, D. and F. T. Haddock, "Antenna Impedance in a Plasma: Problems Relevant to Radio Astronomy Measurements from Space Vehicles", Ann. d'Ap. 28, 605, 1965.

Walsh, D., F. T. Haddock and H. F. Schulte, "Cosmic Radio Intensities at 1.225 and 2.0 Mc Measured up to an Altitude of 1700 km", Space Research, IV, 935, 1964.

Webber, W. R. and C. Chotkowski, "A Determination of the Energy Spectrum of Extraterrestrial Electrons in the Energy Range 70-2000 Mev", J. Geophys. R. 72, 2783, 1967.

Weber, R. R., R. G. Stone and C. R. Somerlock, "Cosmic Radio Noise Intensity from 0.45 to 3.0 MHz Observed by the ATS-II Satellite", to be published, 1968.

(5) Westerhout, Gart, "A Survey of the Continuous Radiation from the Galactic System at a Frequency of 1390 Mc/s", B. A. N. 14, 215, 1958.

Wielebinski, R. and K. W. Yates, "Spectrum of Galactic Radio Emission", Nature 205, 581, 1965.

Yates, K. W. and R. Wielebinski, "Sky Brightness at 14.1 Mc/s", Nature 208, 64, 1965.

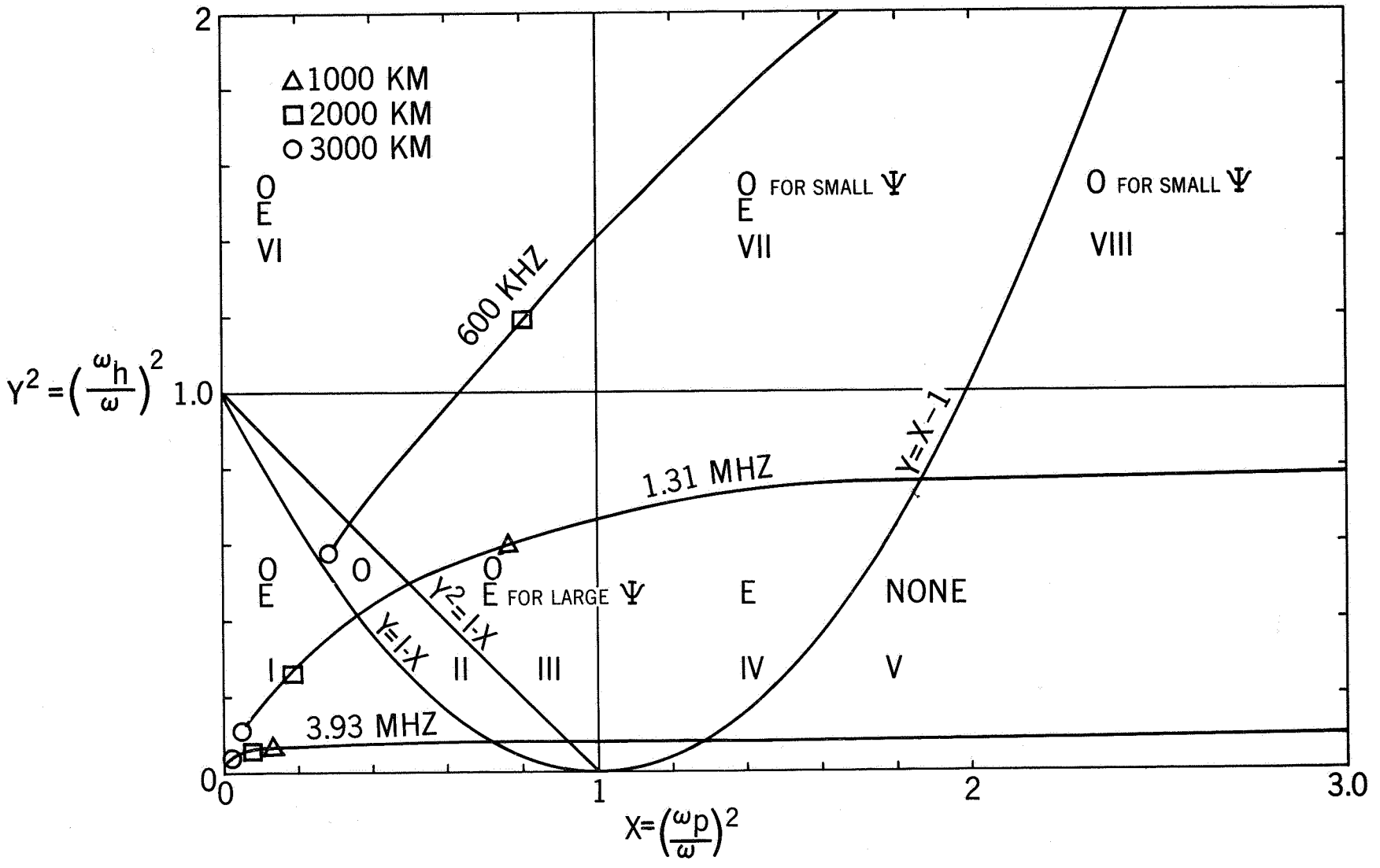

Figure 1. $X\text{-}Y^2$ diagram showing propagation of ordinary (O) or extraordinary (E) wave in each region. The lines labeled 600 kHz, 1.31 MHz and 3.93 MHz indicate the expected trajectory in the diagram at each frequency as a function of altitude for a Wallops Island launch.

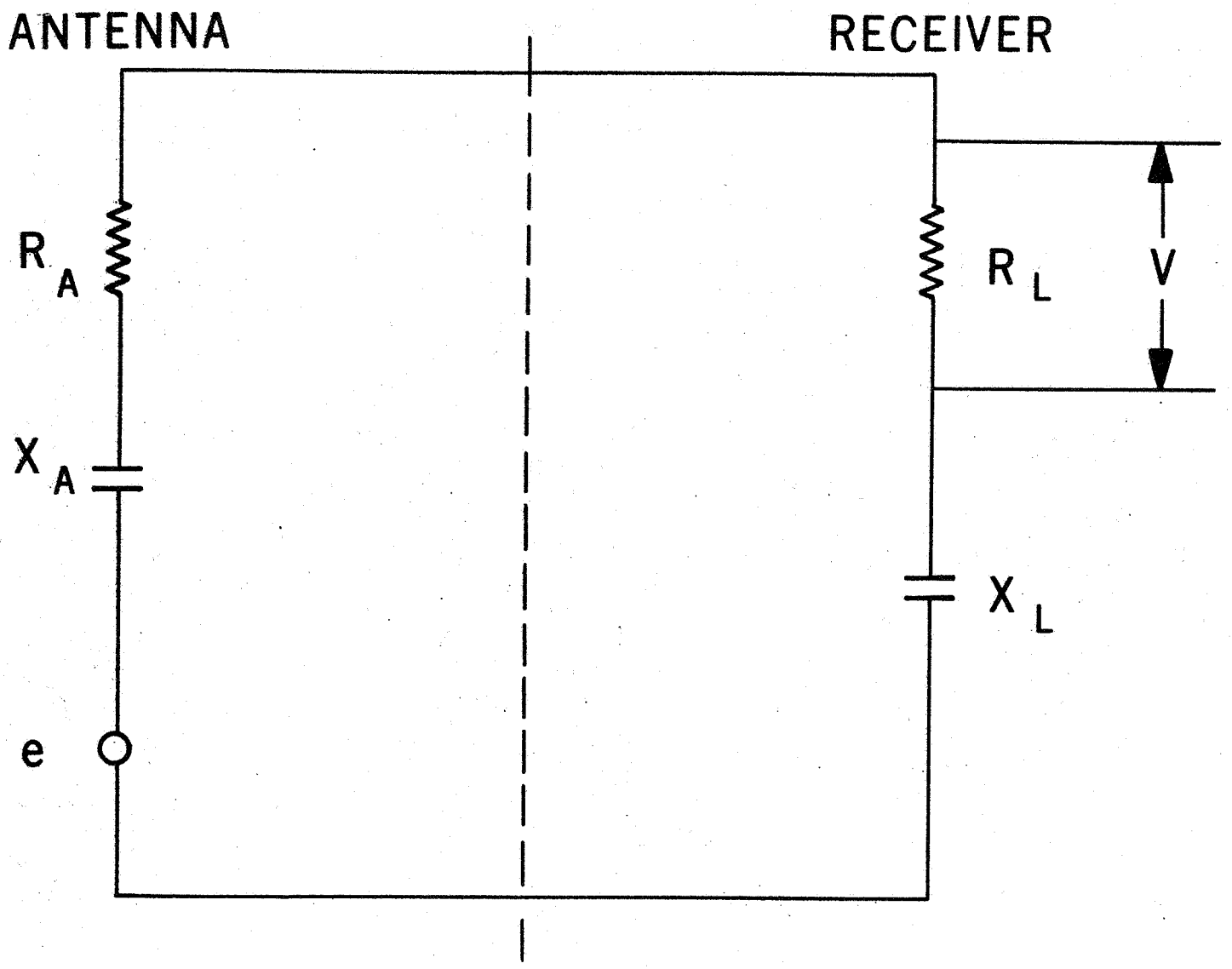

Figure 2. Equivalent circuit for antenna and receiver.

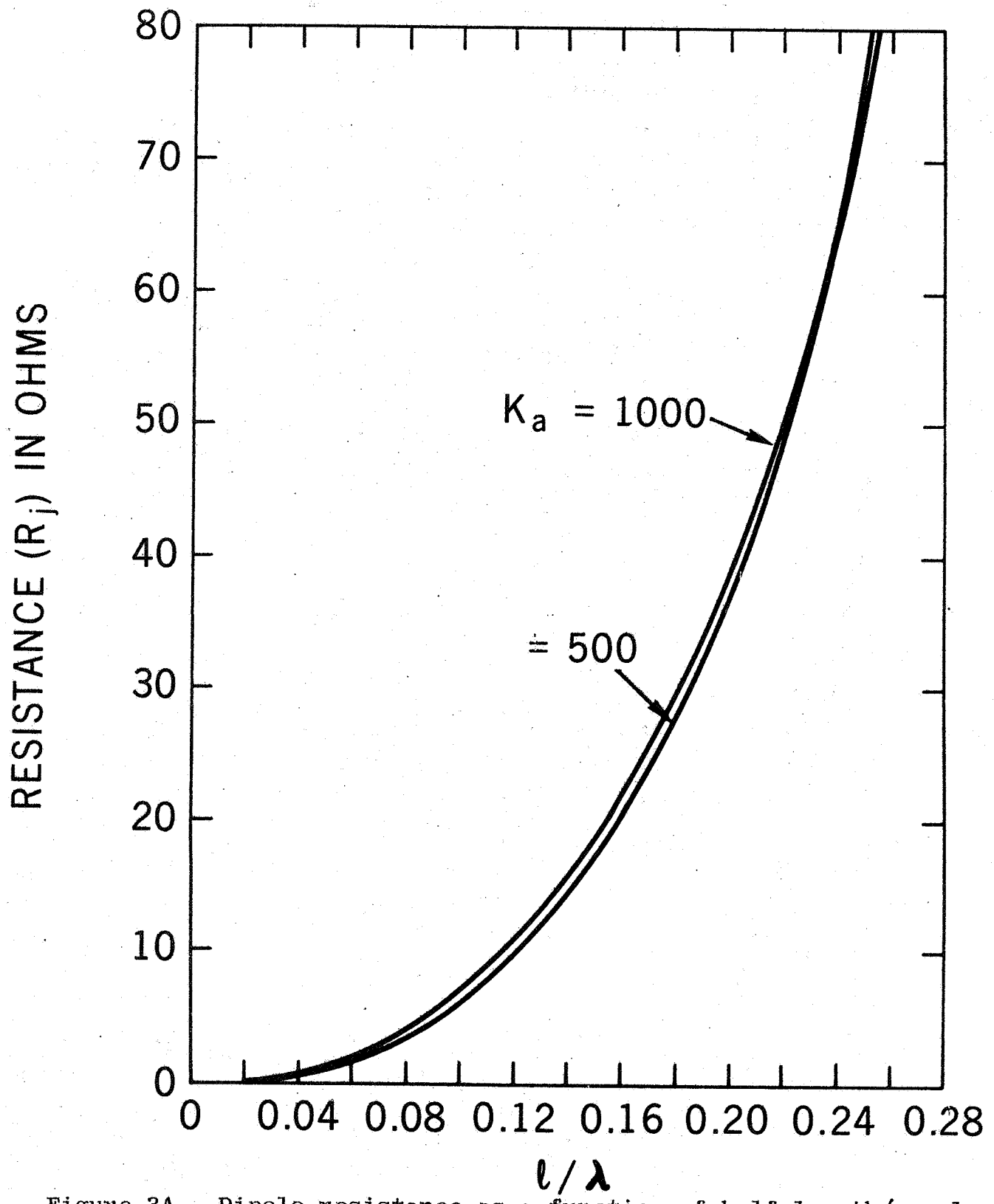

Figure 3A. Dipole resistance as a function of half length/wavelength The thickness parameter $K_a = 120 \log 2\ell/a$ where a is the radius of the antenna.

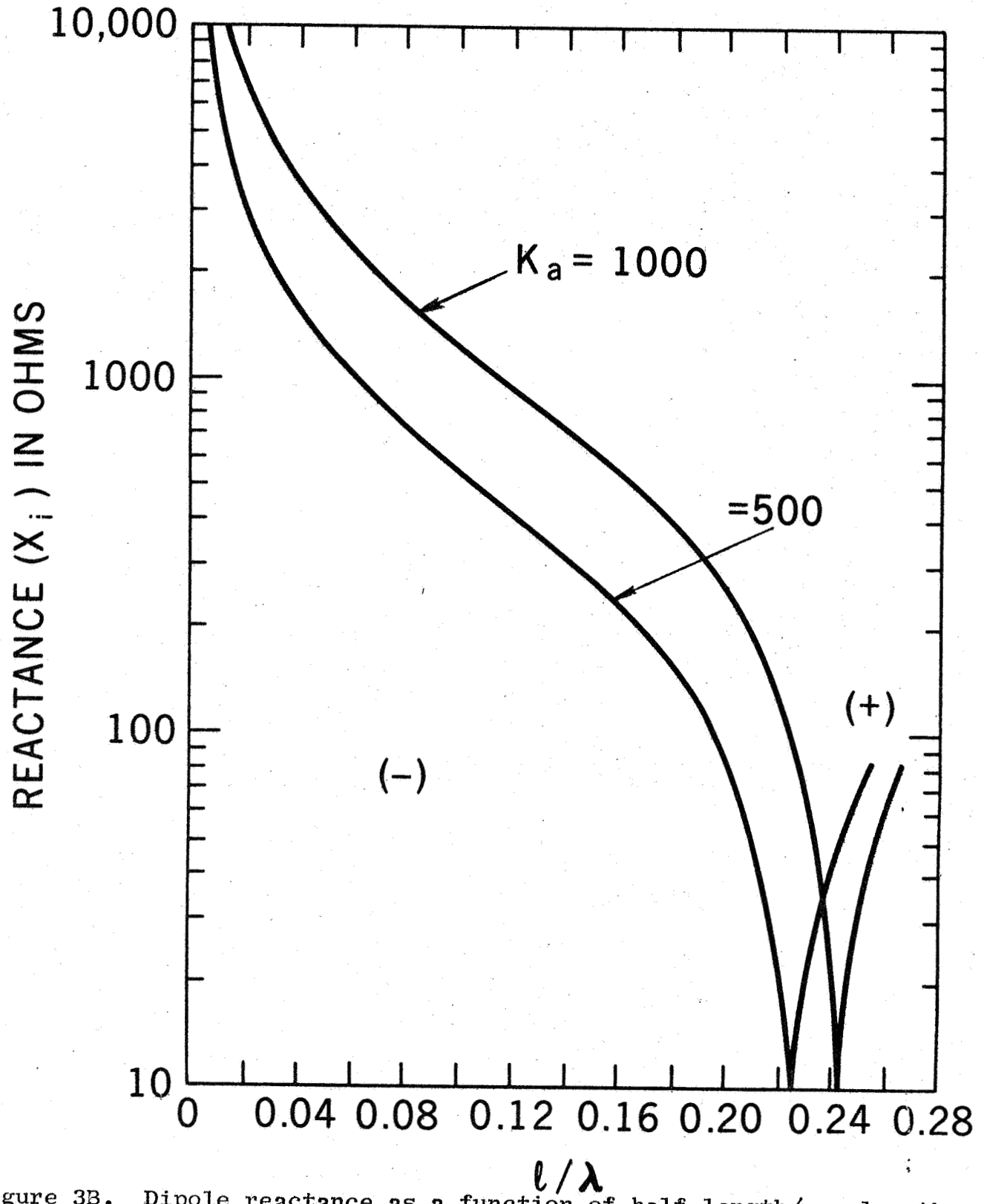

Figure 3B. Dipole reactance as a function of half length/wavelength The thickness parameter K_a = 120 log $2\ell/a$ where a is the radius of the antenna.

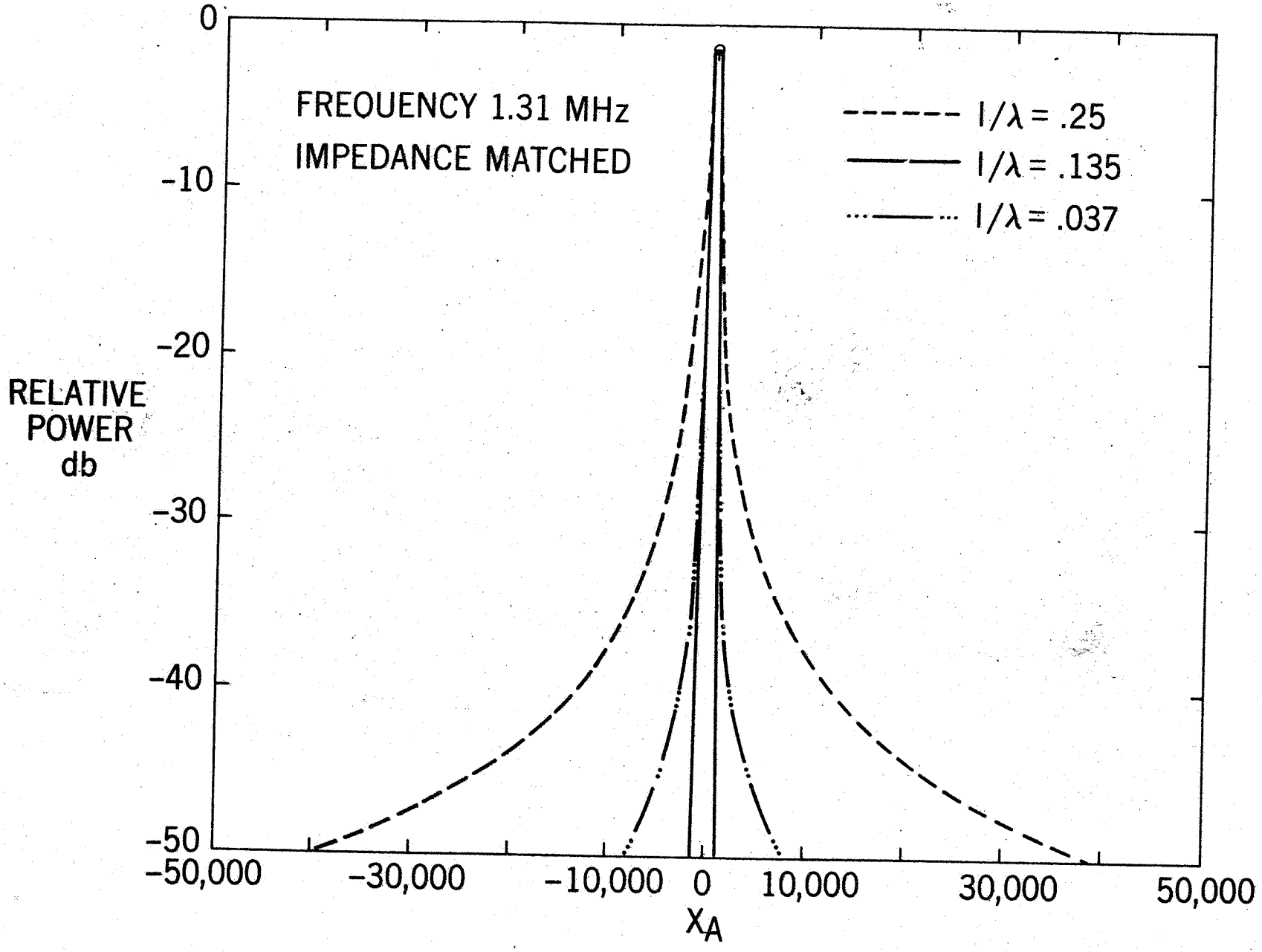

Figure 4. Variation of received power with antenna reactance for a matched receiver and several antenna lengths.

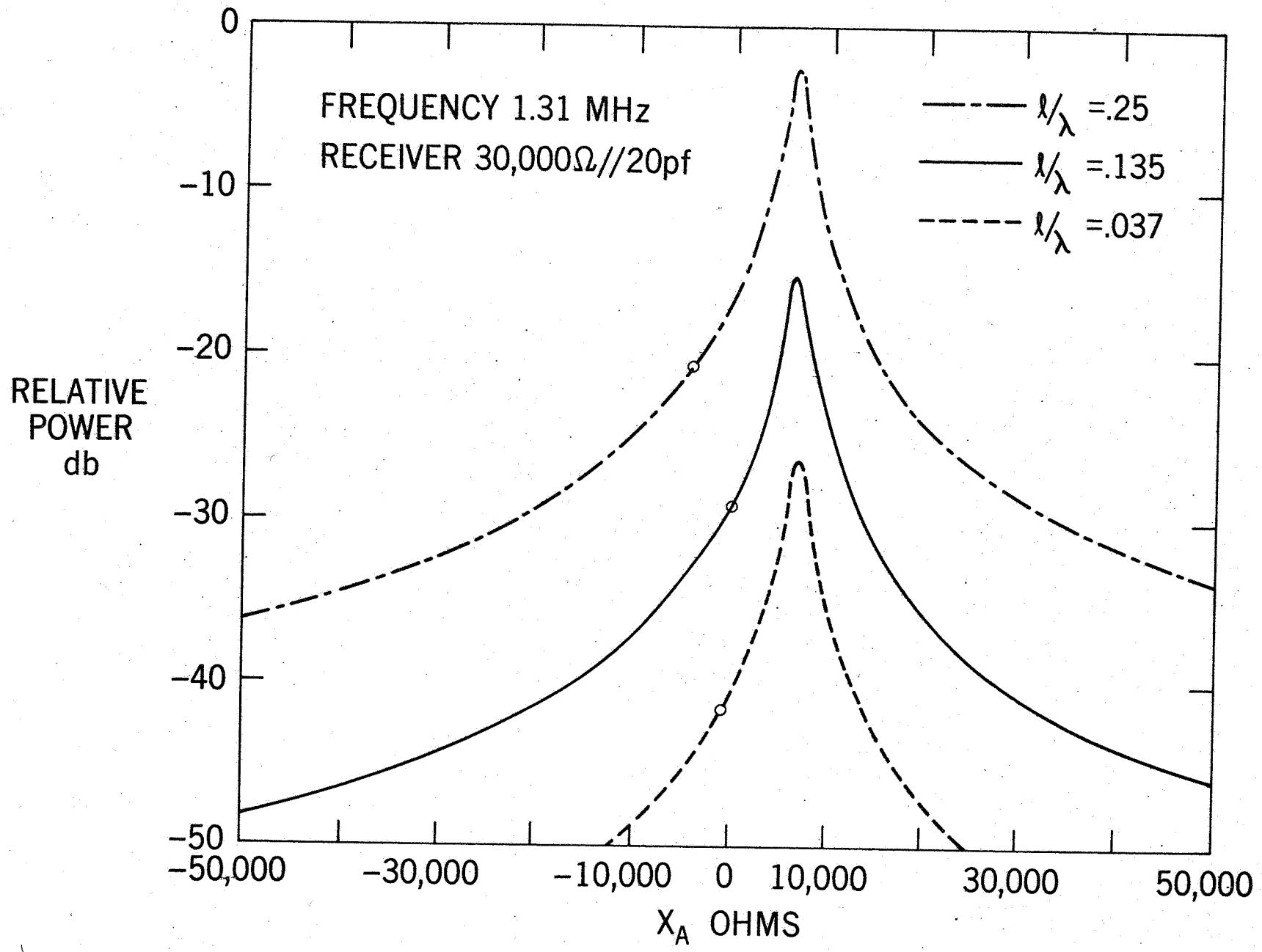

Figure 5. Variation of received power with antenna reactance for a high impedance receiver and several antenna lengths.

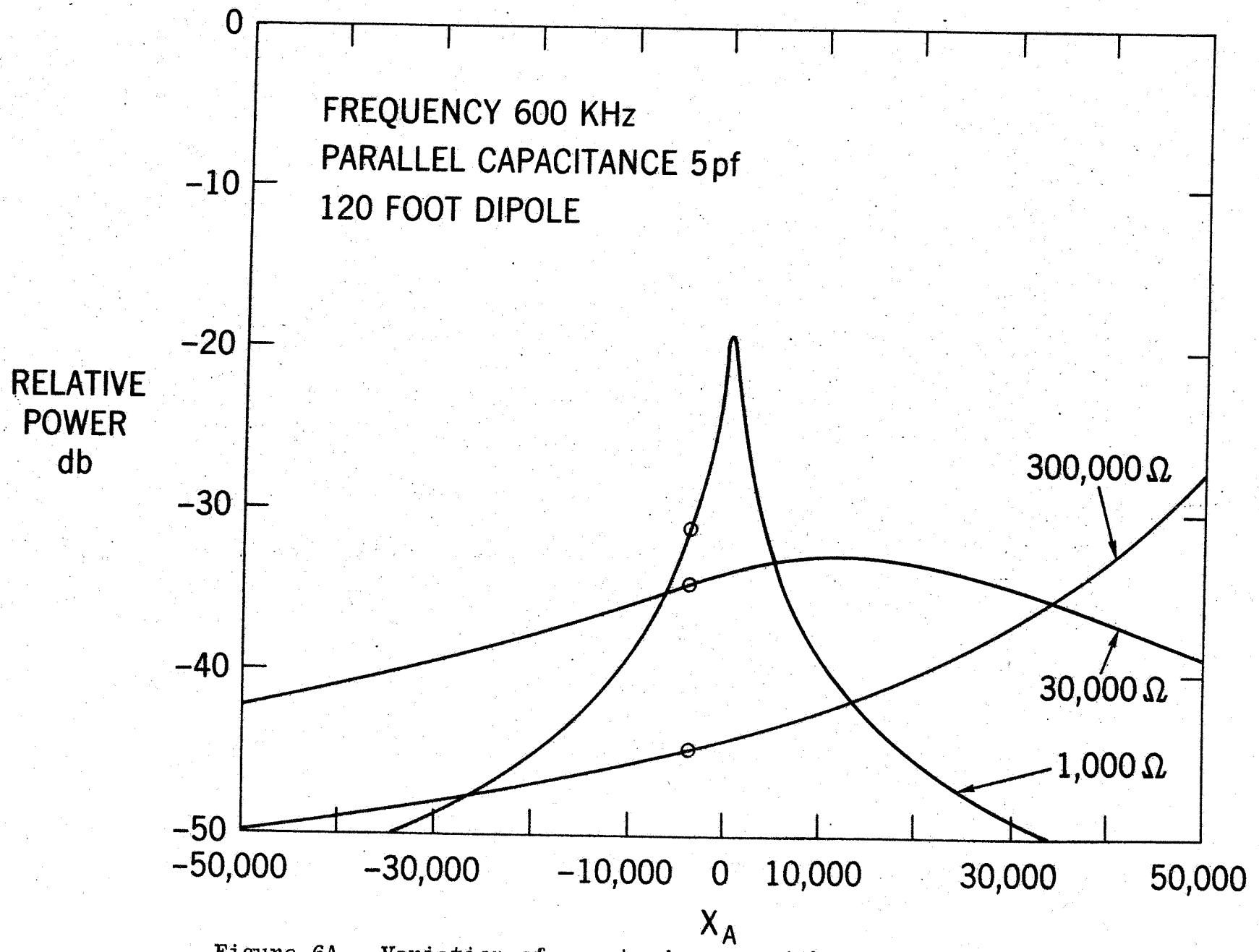

Figure 6A. Variation of received power with antenna reactance for a receiver of 5 pf in parallel with several resistances.

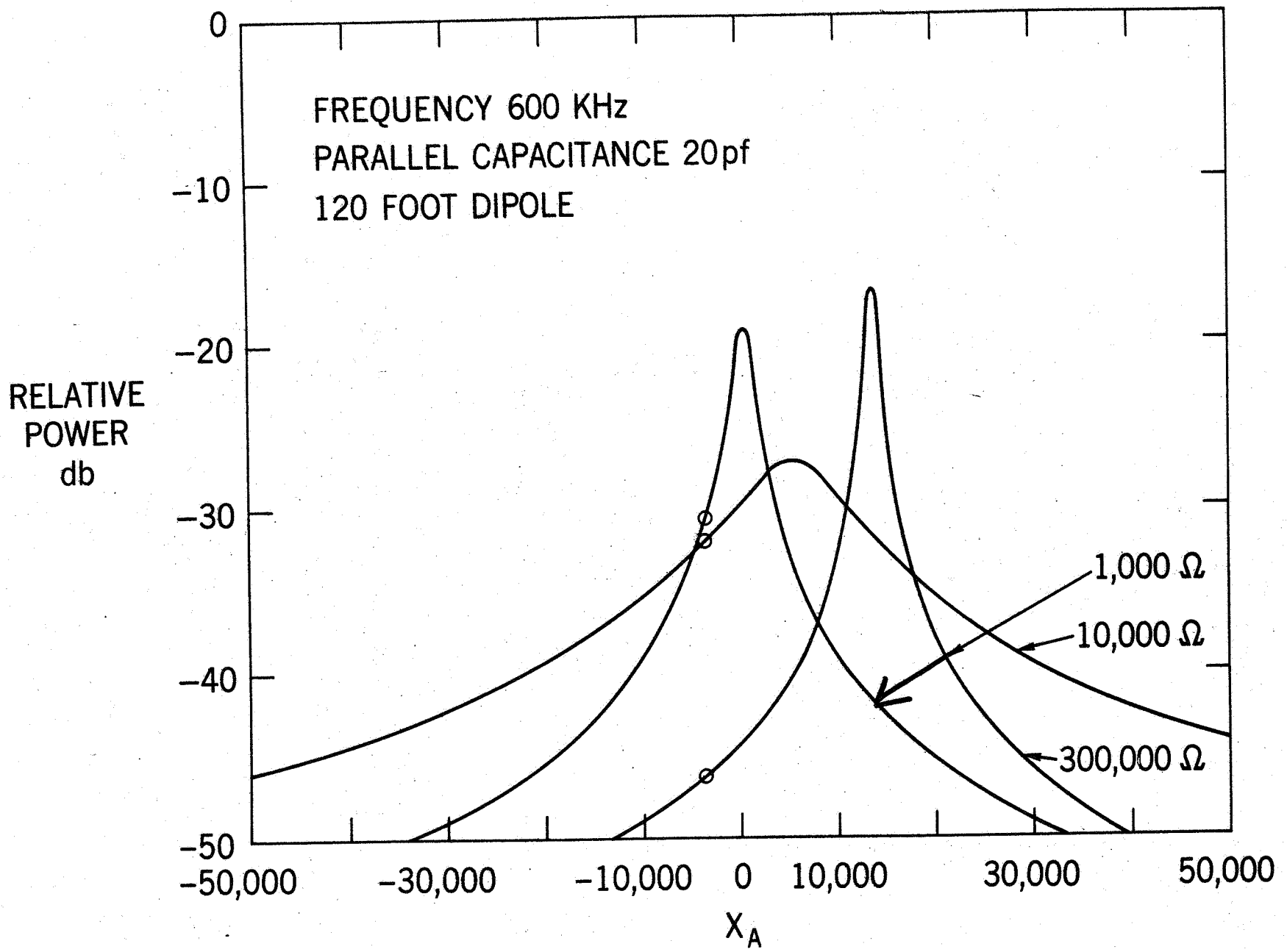

Figure 6B. Variation of received power with antenna reactance for a receiver of 20 pf in parallel with several resistances.

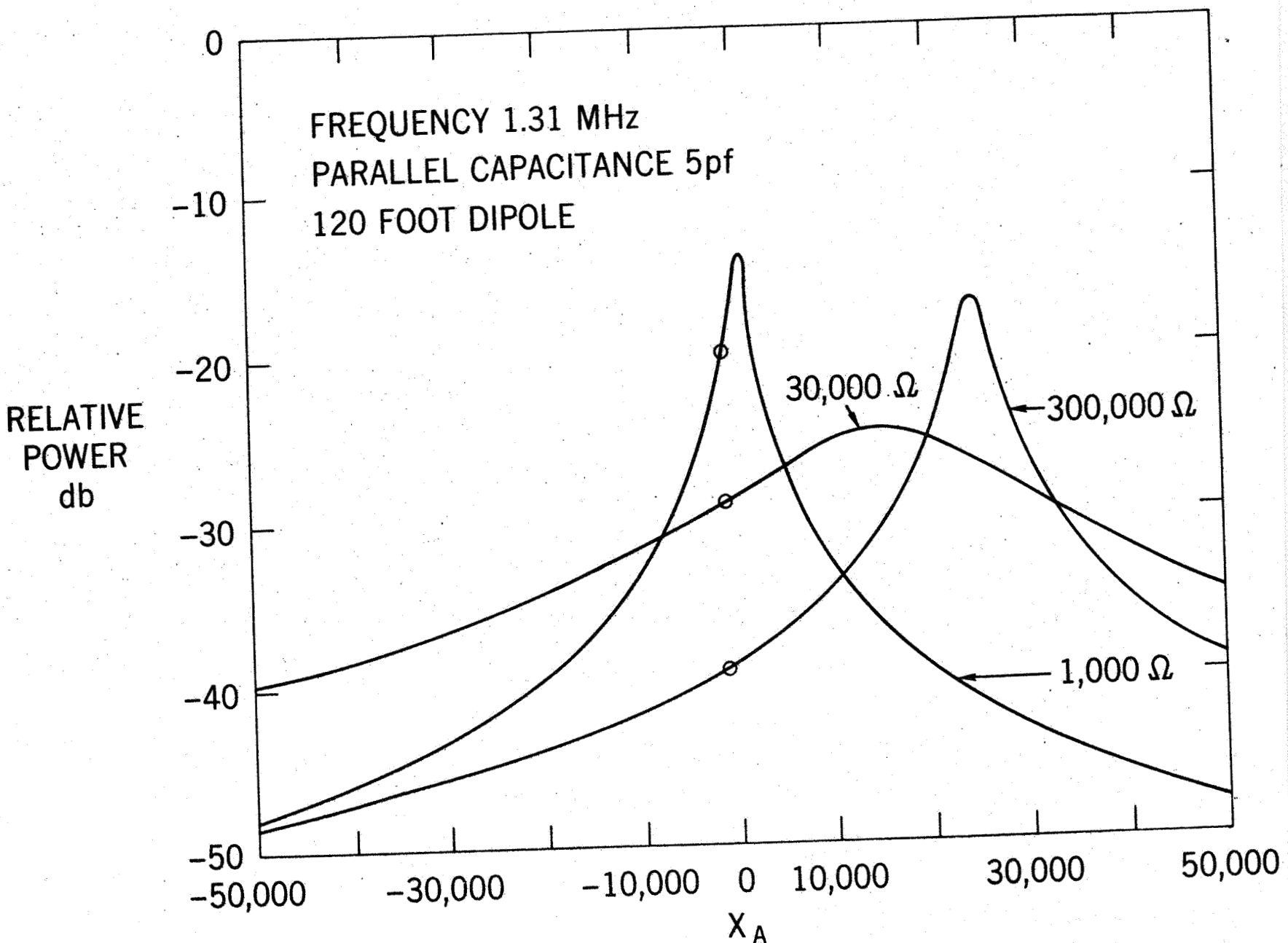

Figure 6C. Variation of received power with antenna reactance for a receiver of 5 pf in parallel with several resistances.

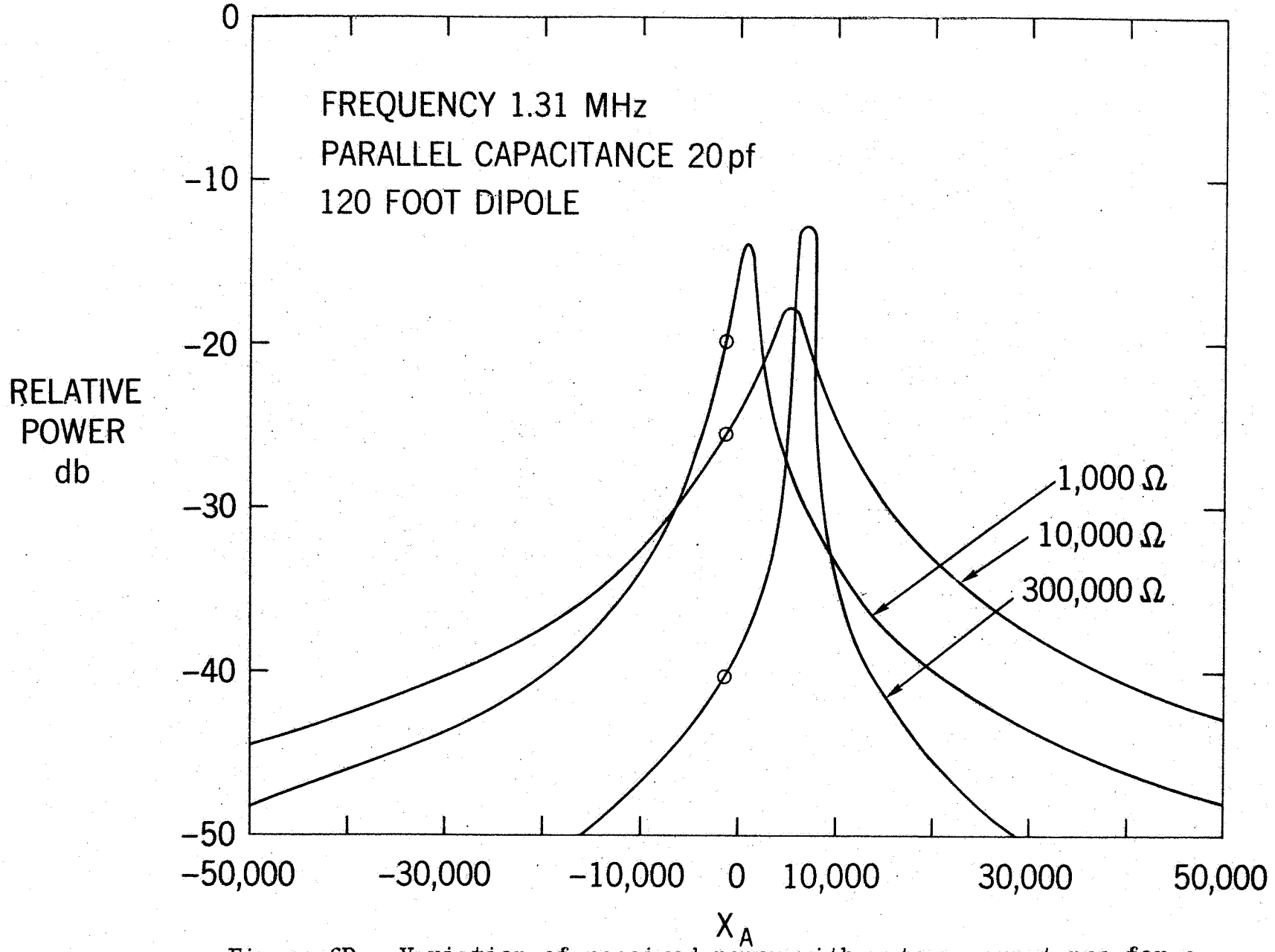

Figure 6D. Variation of received power with antenna reactance for a receiver of 20 pf in parallel with several resistances.

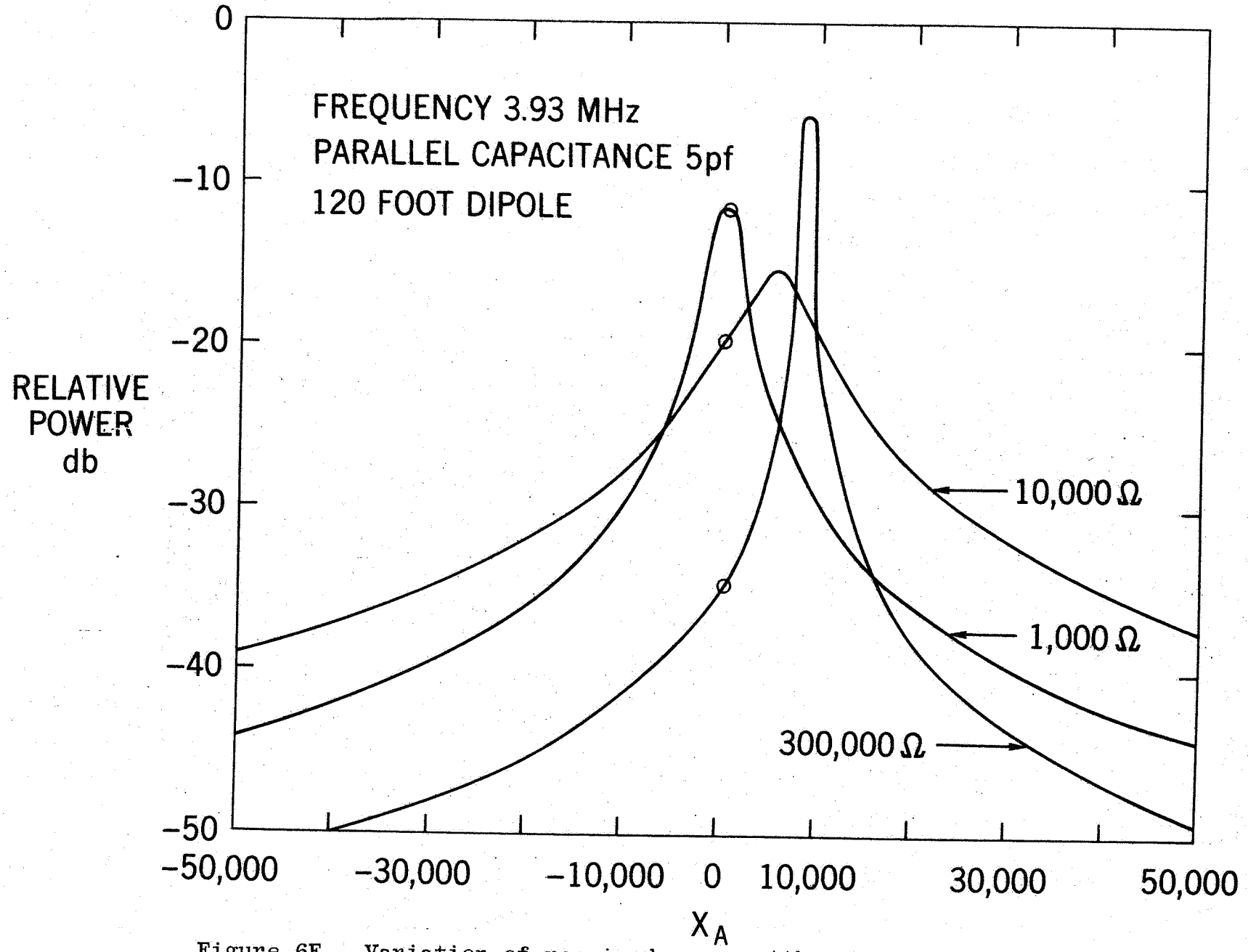

Figure 6E. Variation of received power with antenna reactance for a receiver of 5 pf in parallel with several resistances.

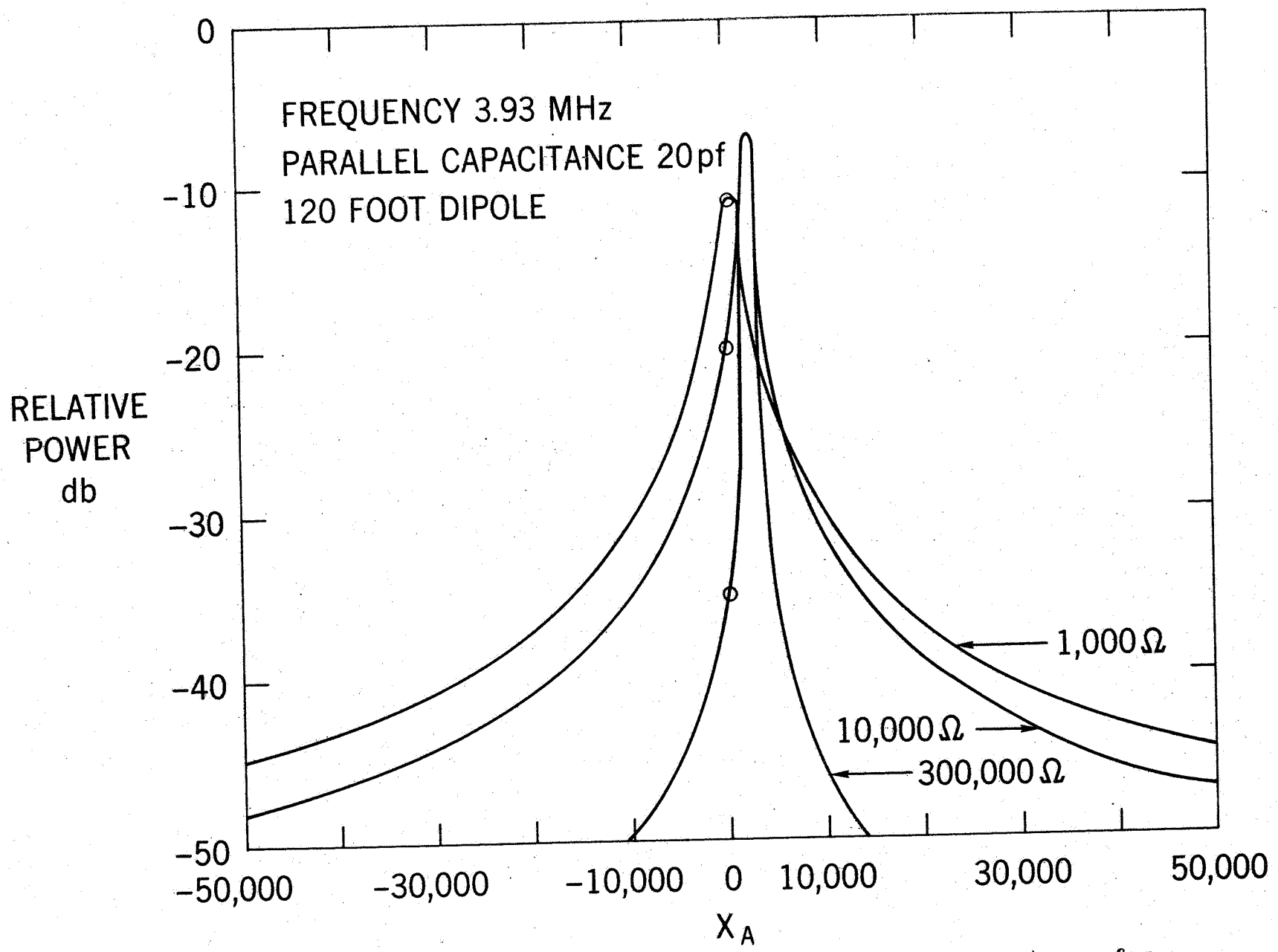

Figure 6F. Variation of received power with antenna reactance for a receiver of 20 pf in parallel with several resistances.

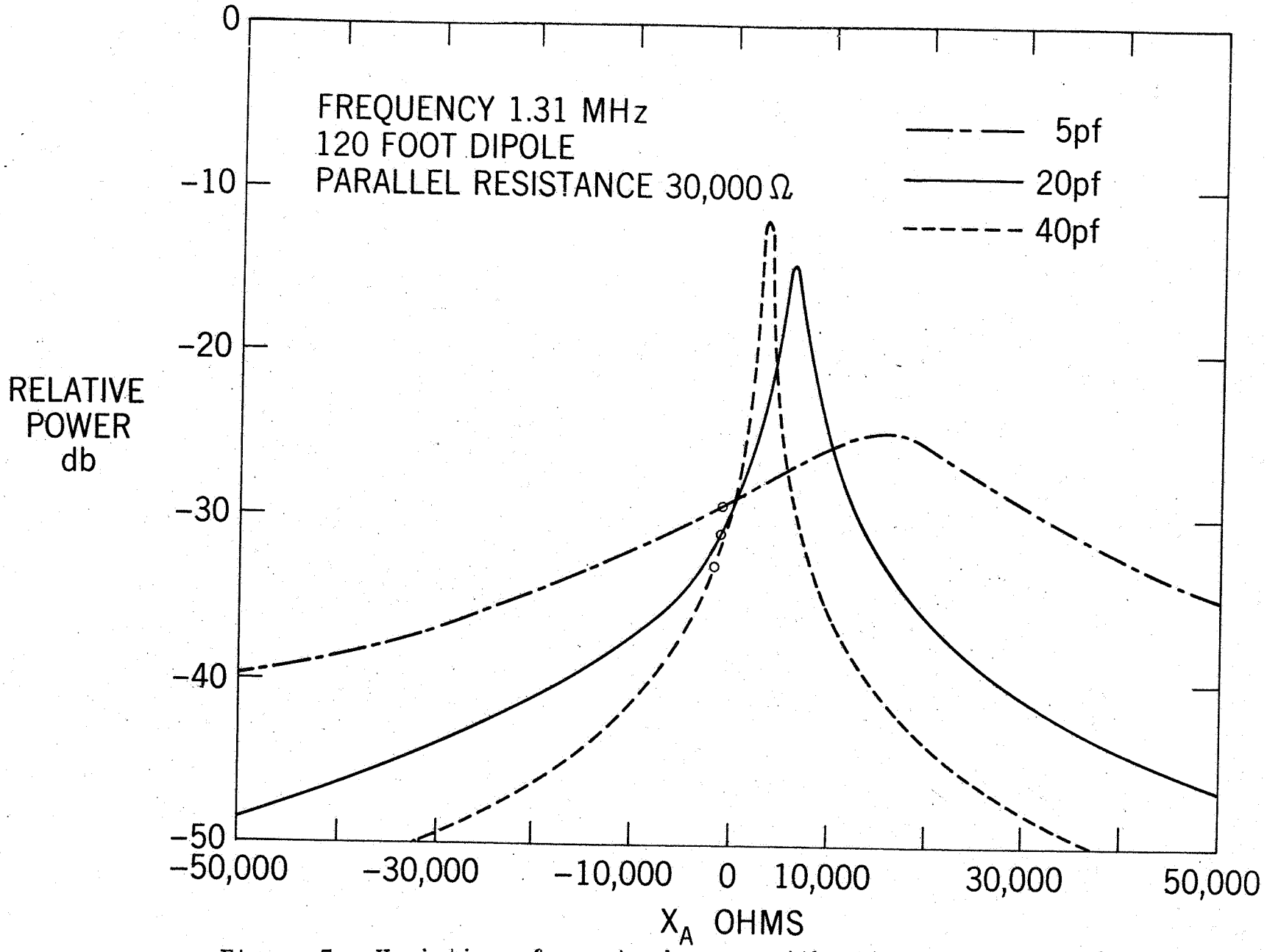

Figure 7. Variation of received power with antenna reactance for a receiver of 30,000Ω in parallel with several capacitances.

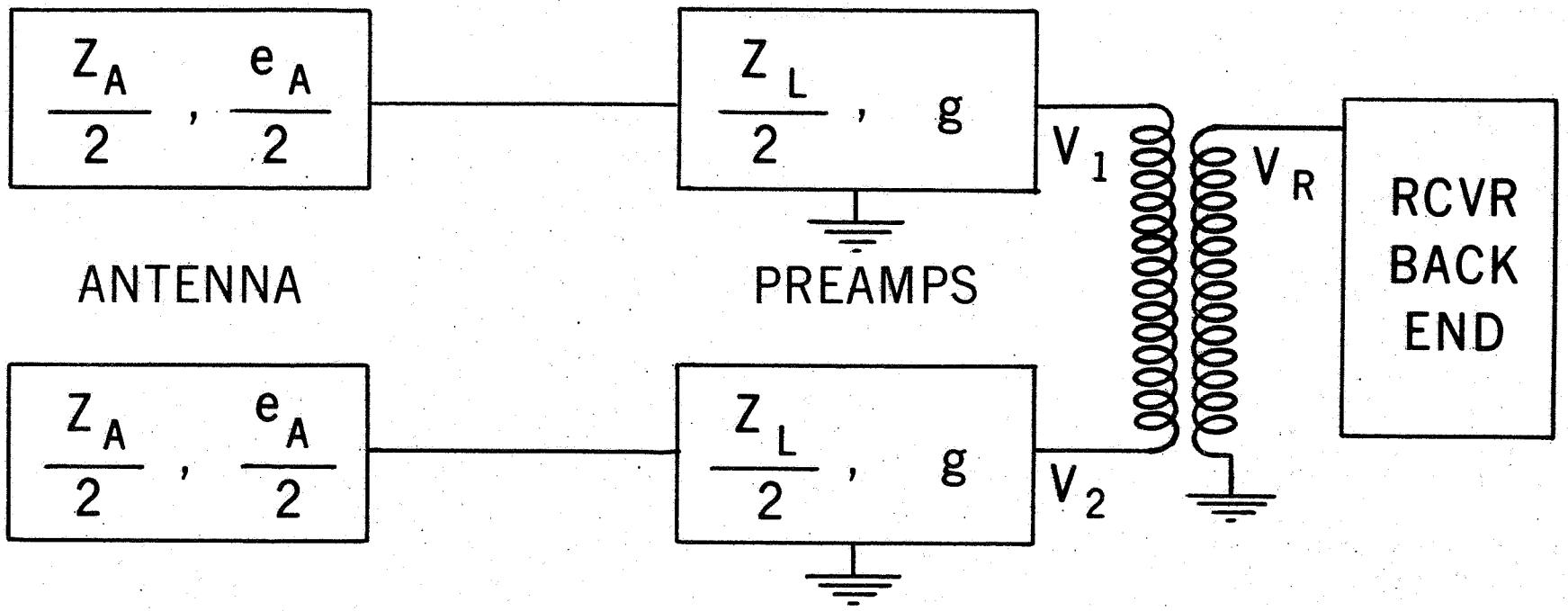

Figure 8. Circuit for antenna and receiver showing the two sides separately.

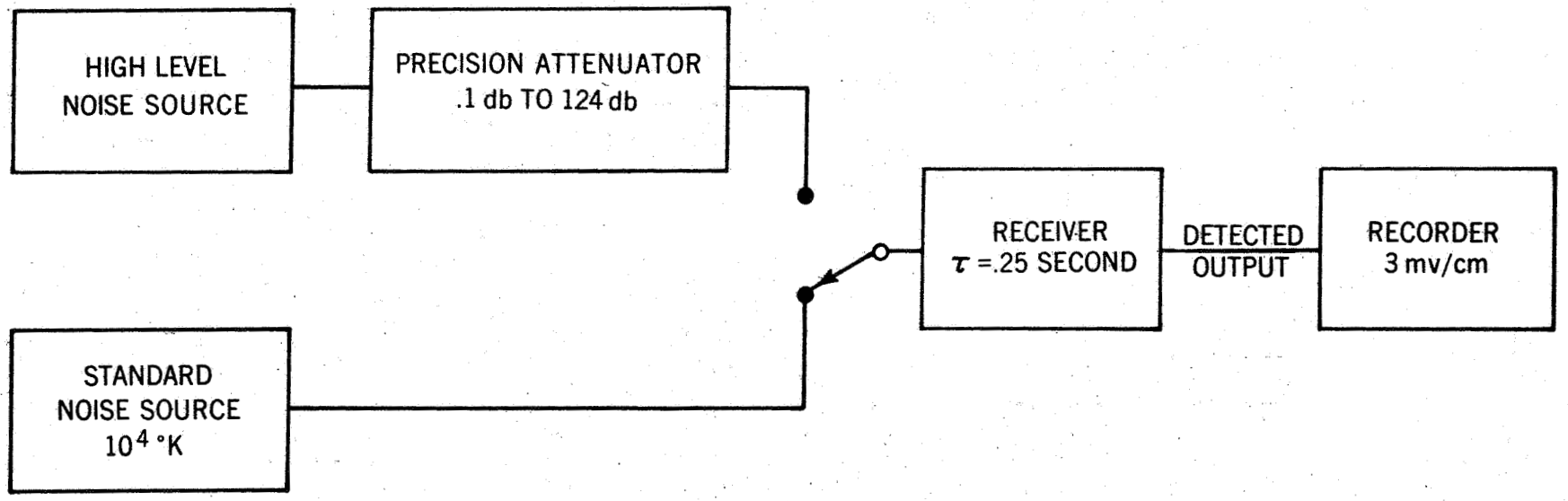

Figure 9. Calibration of high level noise source by comparing with standard noise source.

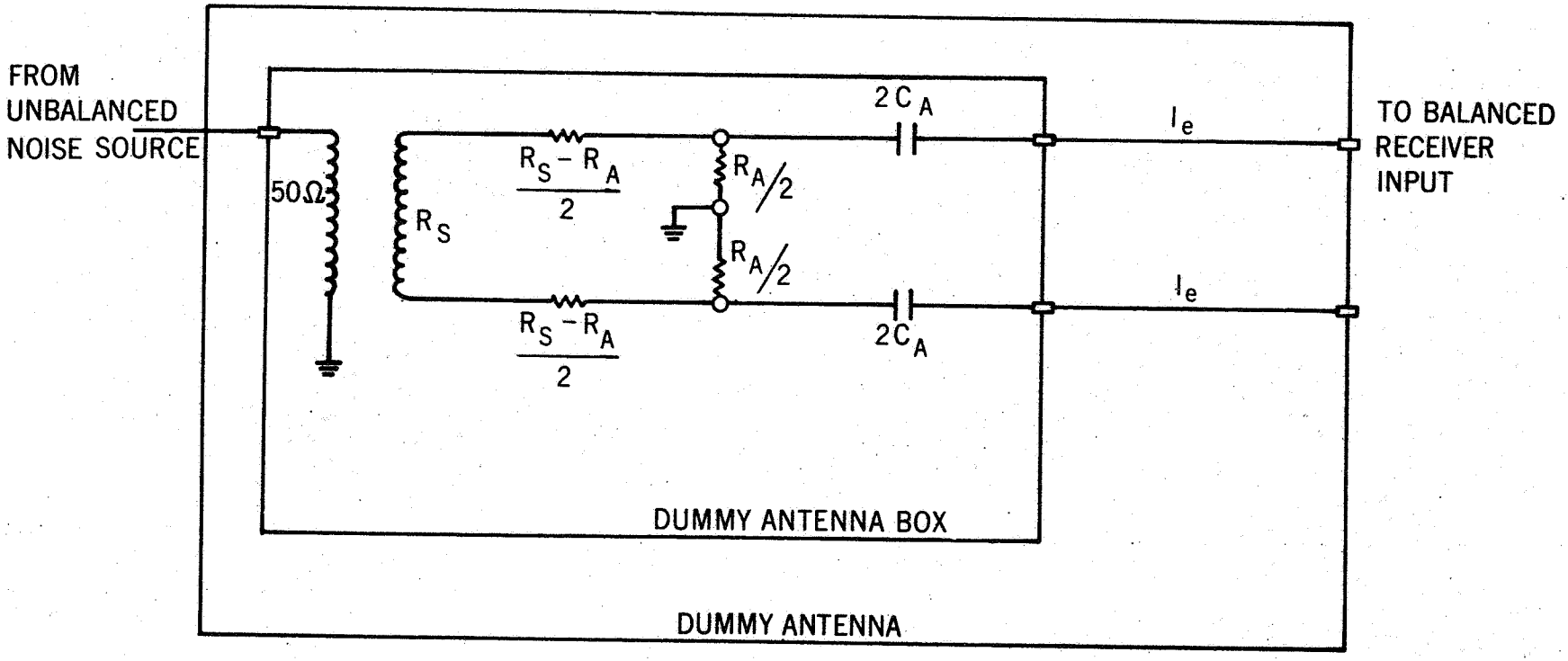

Figure 10. Dummy antenna including cables to spacecraft.

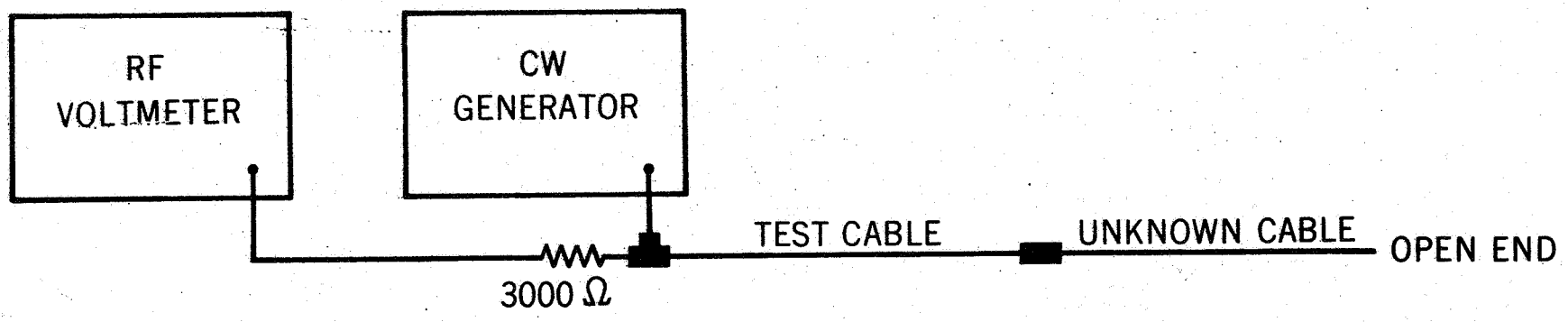

Figure 11. Electrical length measurement. The voltmeter reads a minimum when the test plus unknown cables are $(2n-1)/\lambda$ in length, n = 1,2,3. . .

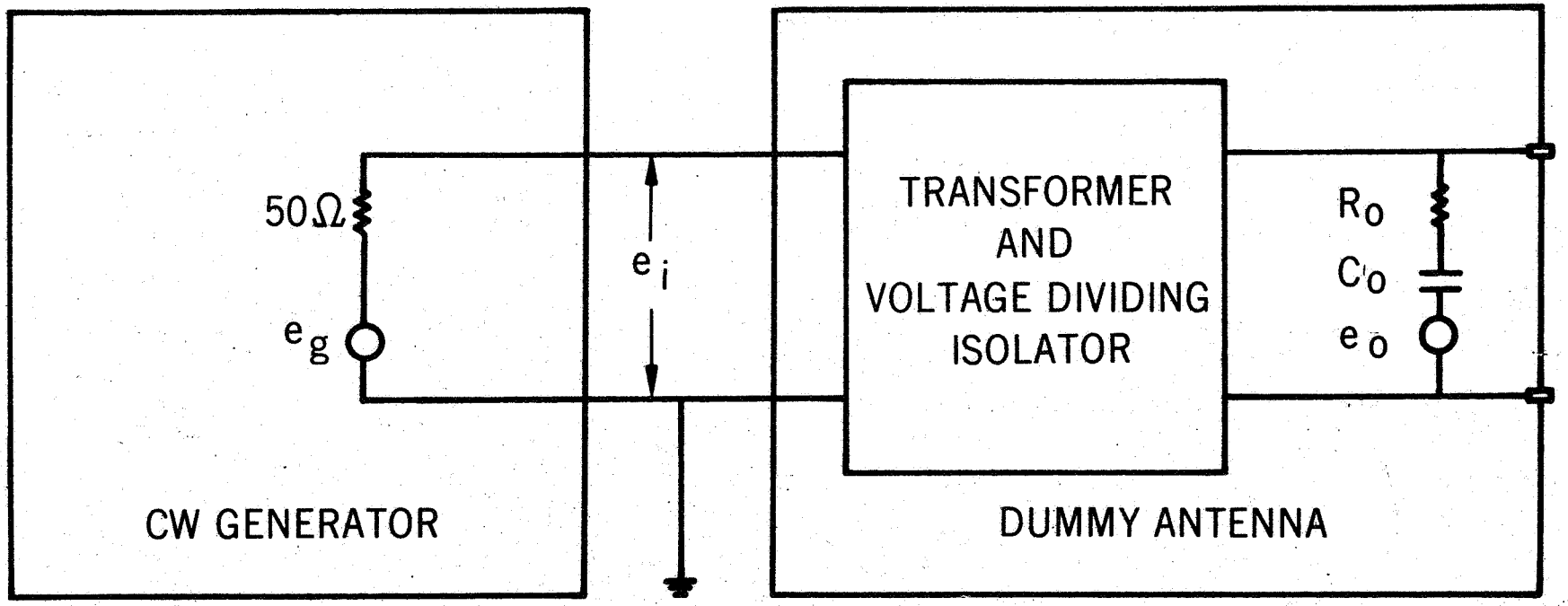

Figure 12. Measurement of dummy antenna characteristics

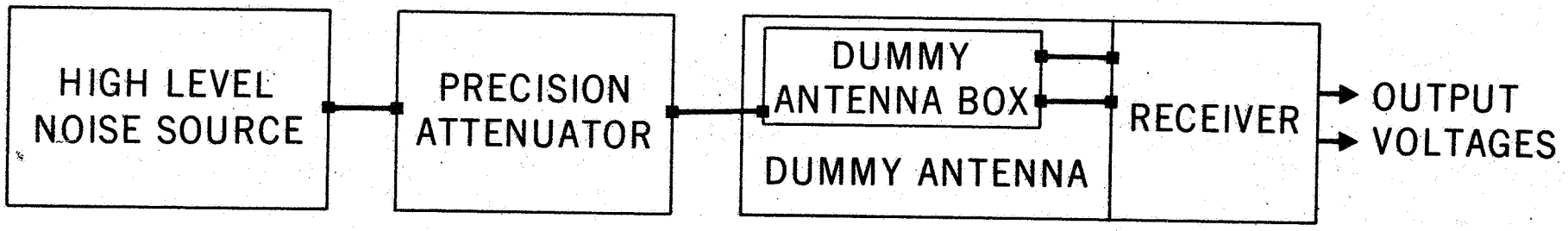

Figure 13. Receiver calibration block diagram.

REPRODUCIBILITY OF THE
ORIGINAL PAGE IS POOR

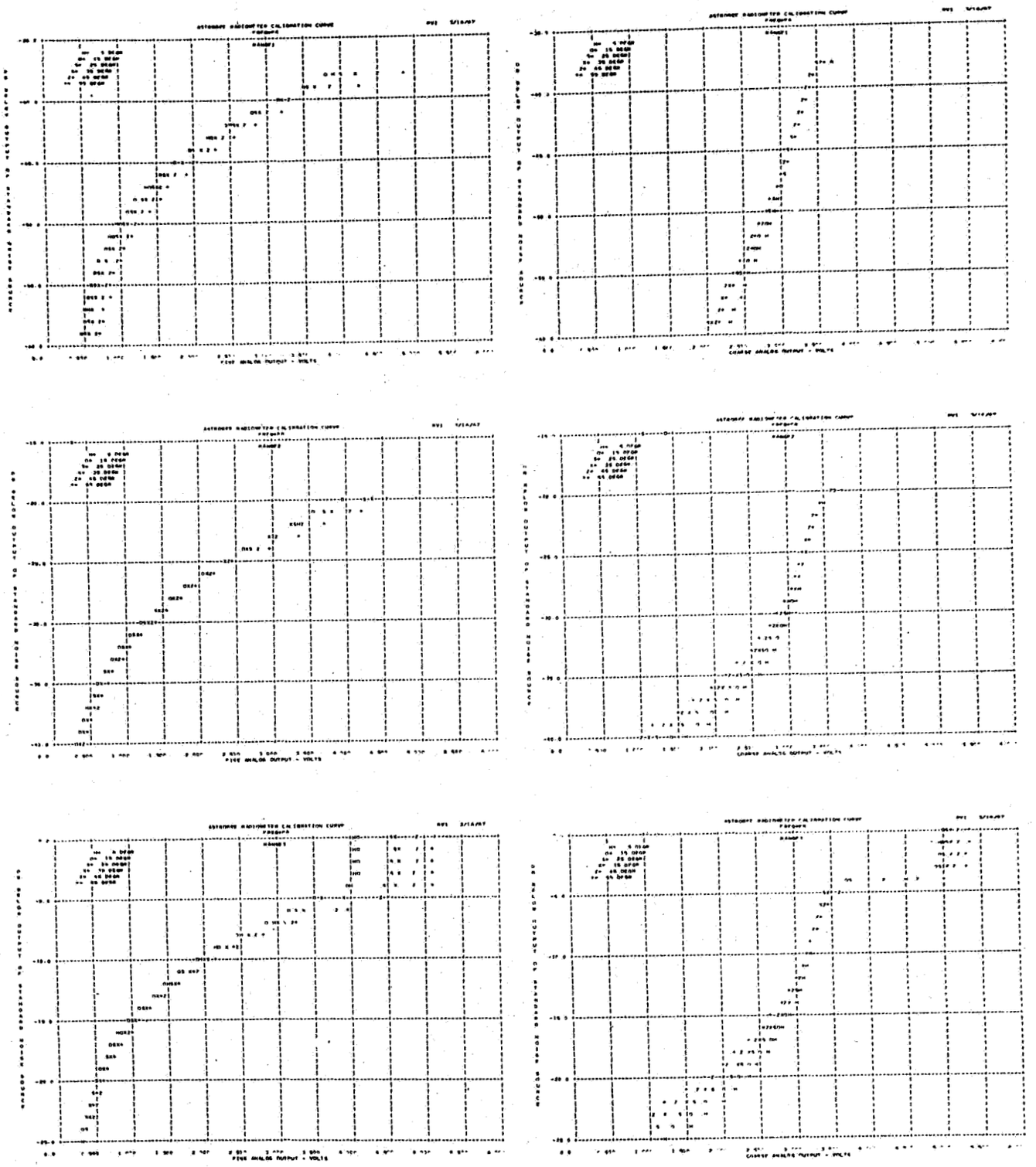

Figure 14. Automatic computer plotting of Ryle Vonberg calibration curves.

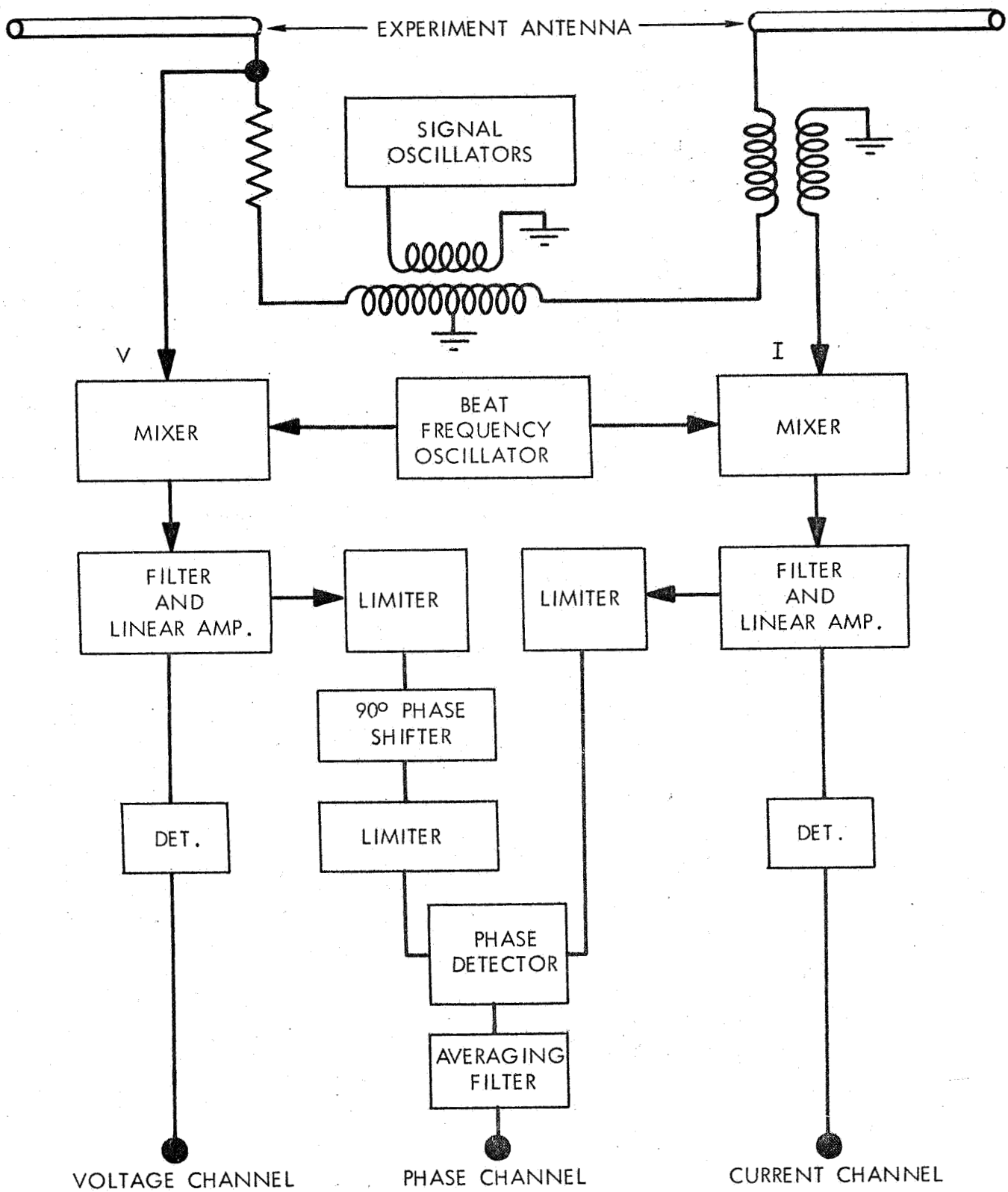

Figure 15. Impedance probe block diagram.

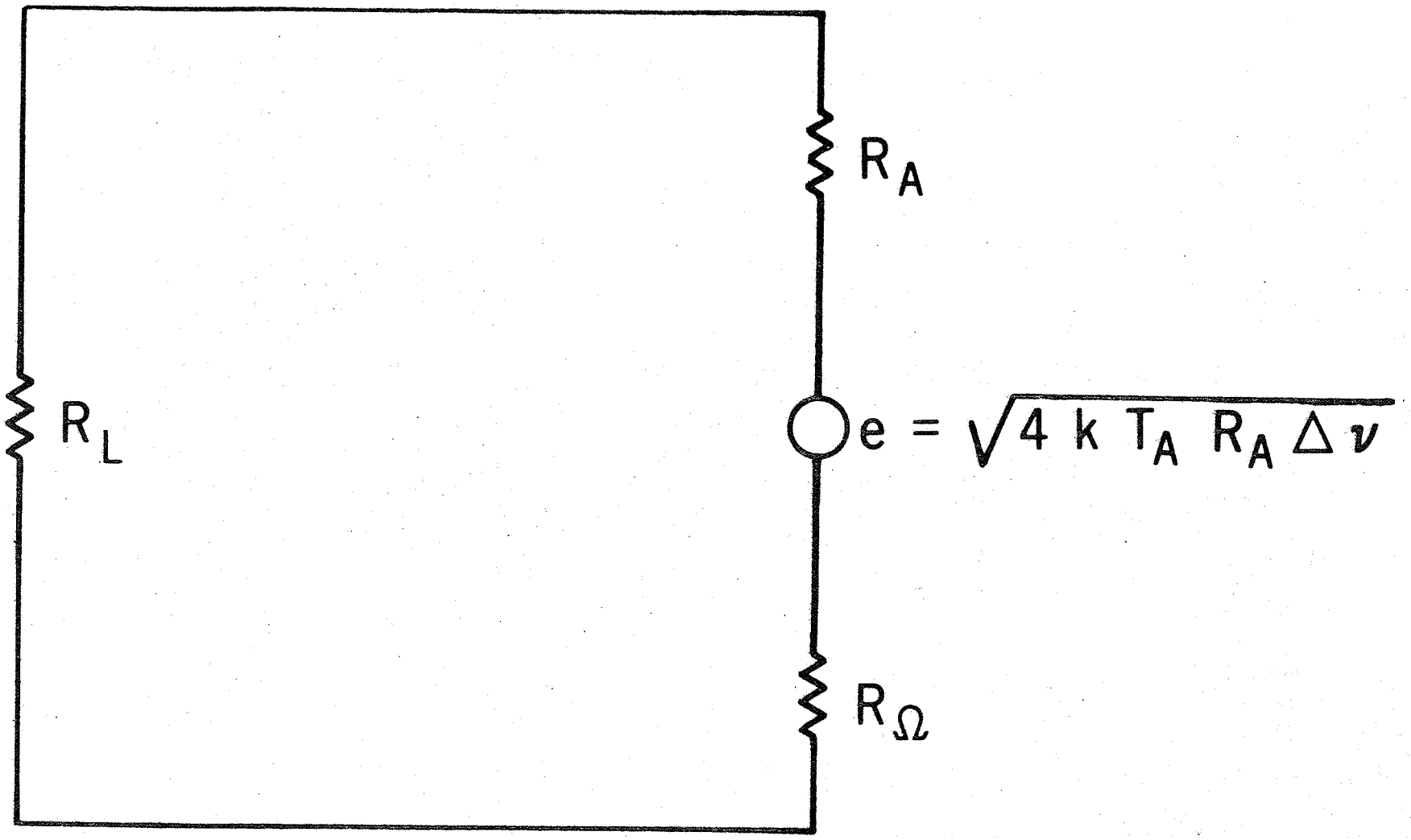

Figure 16. Equivalent circuit for antenna and receiver, neglecting reactances.

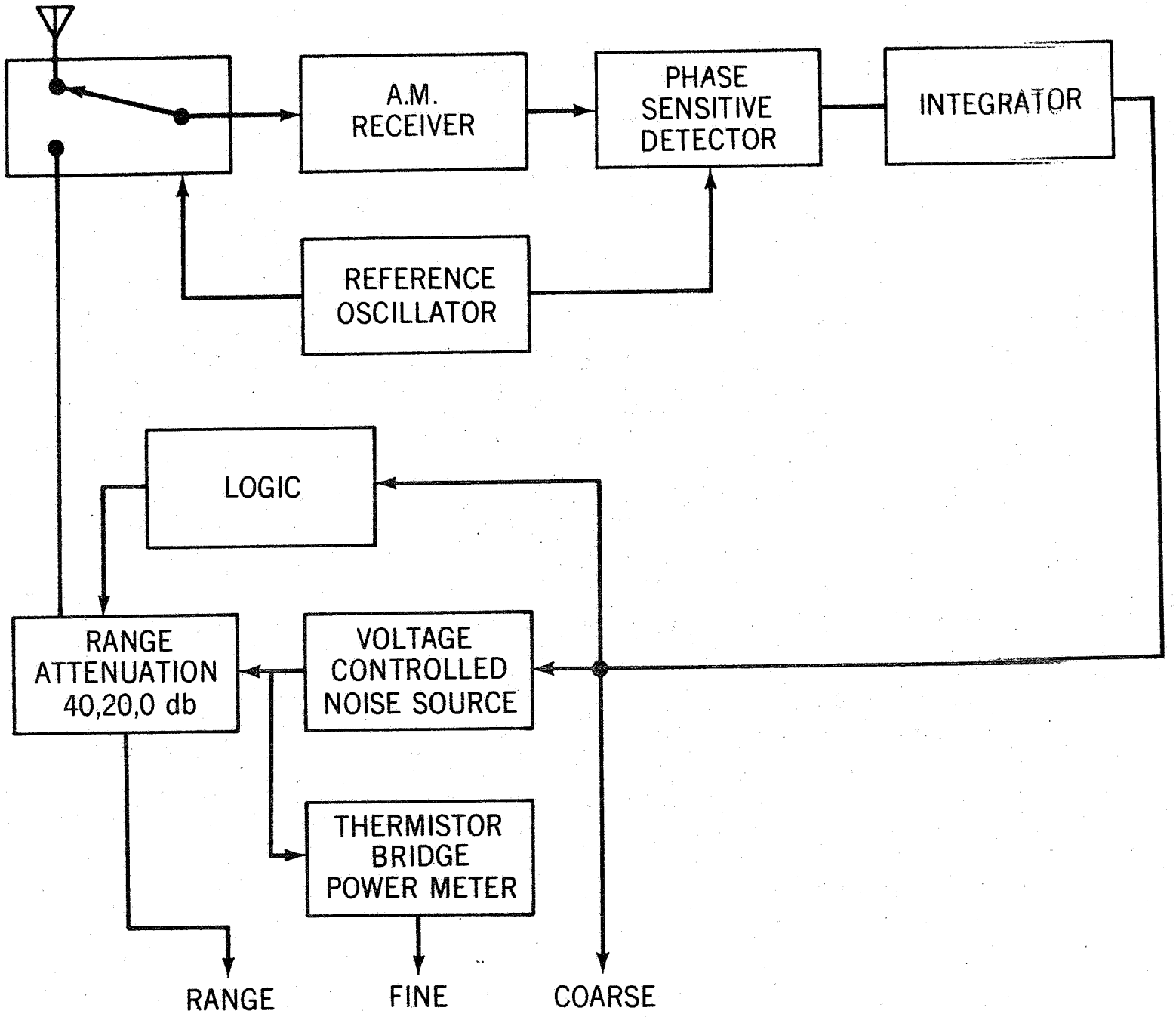

Figure 17. GSFC Ryle Vonberg receiver block diagram.

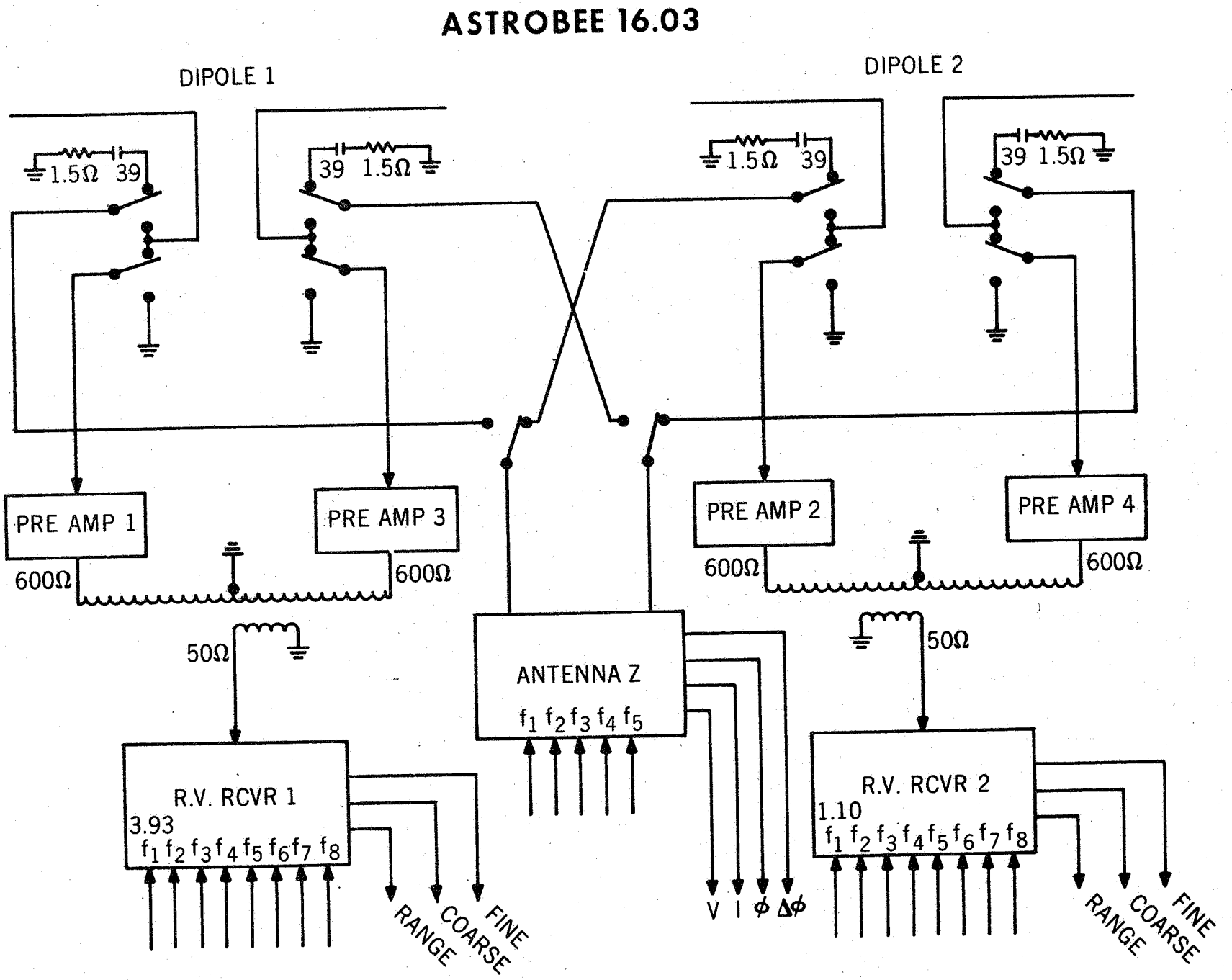

Figure 18. Astrobee 16.03 experiment block diagram.

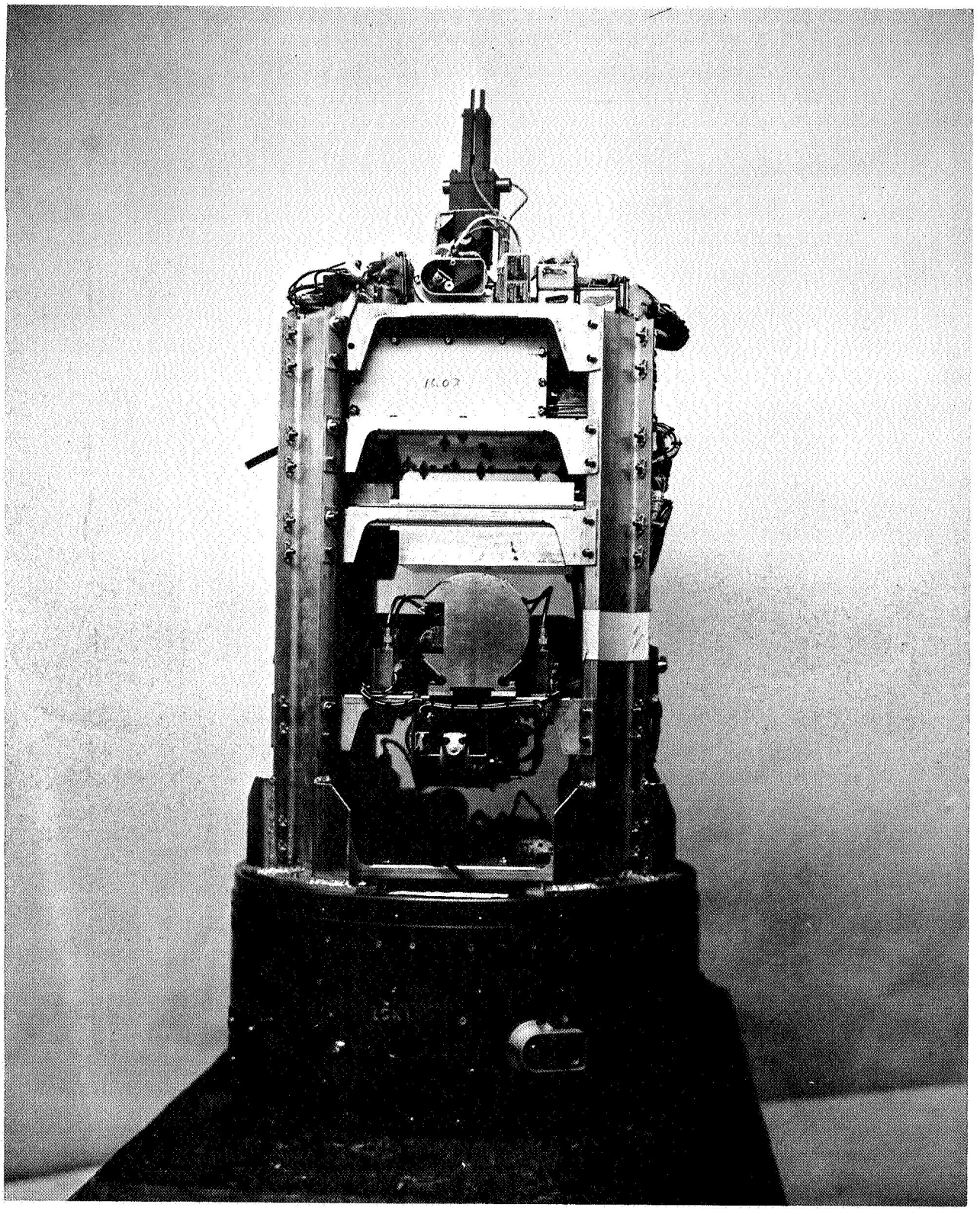

Figure 19. Astrobee 16.03 payload

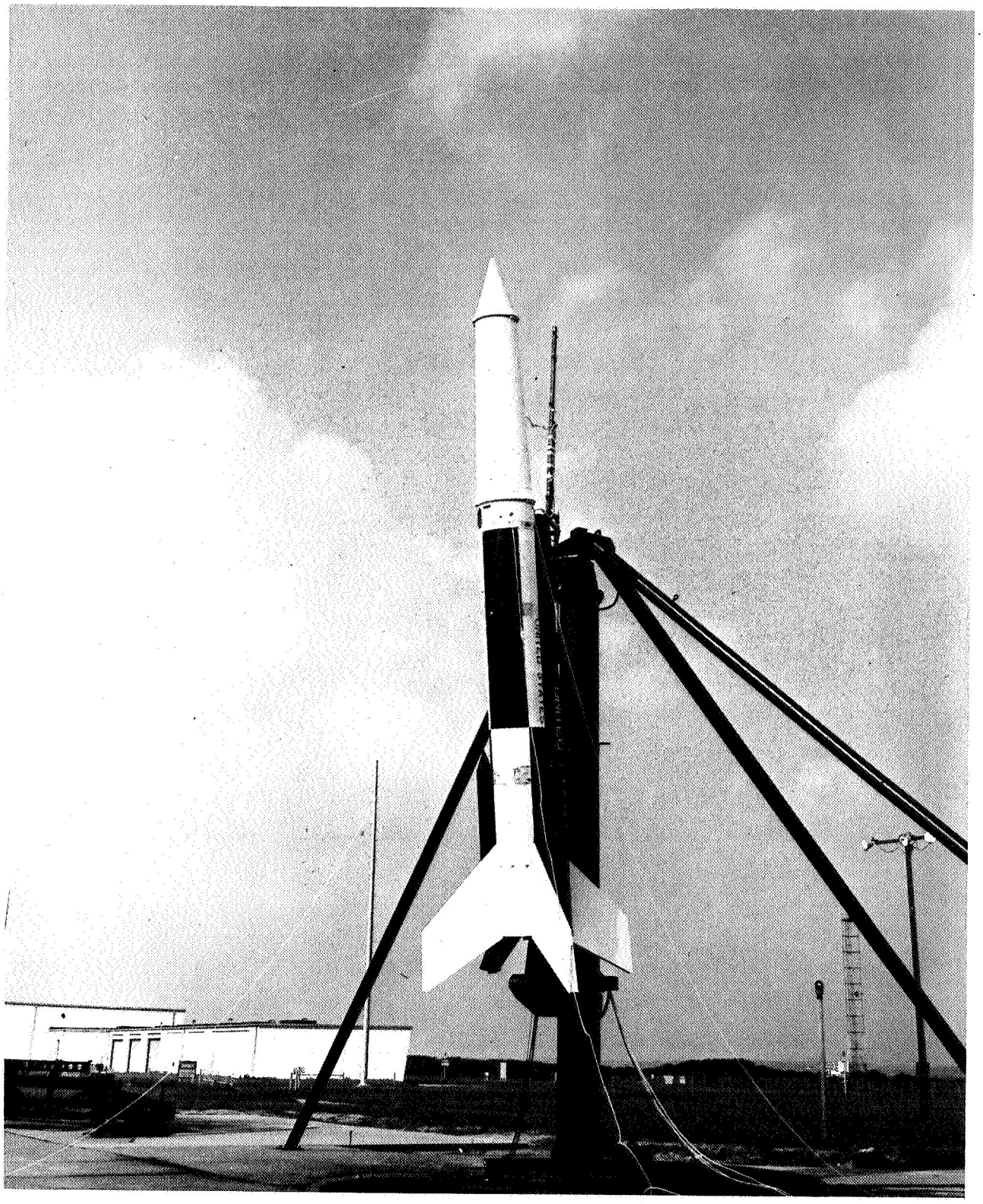

Figure 20. Astrobee 16.03 on launch pad.

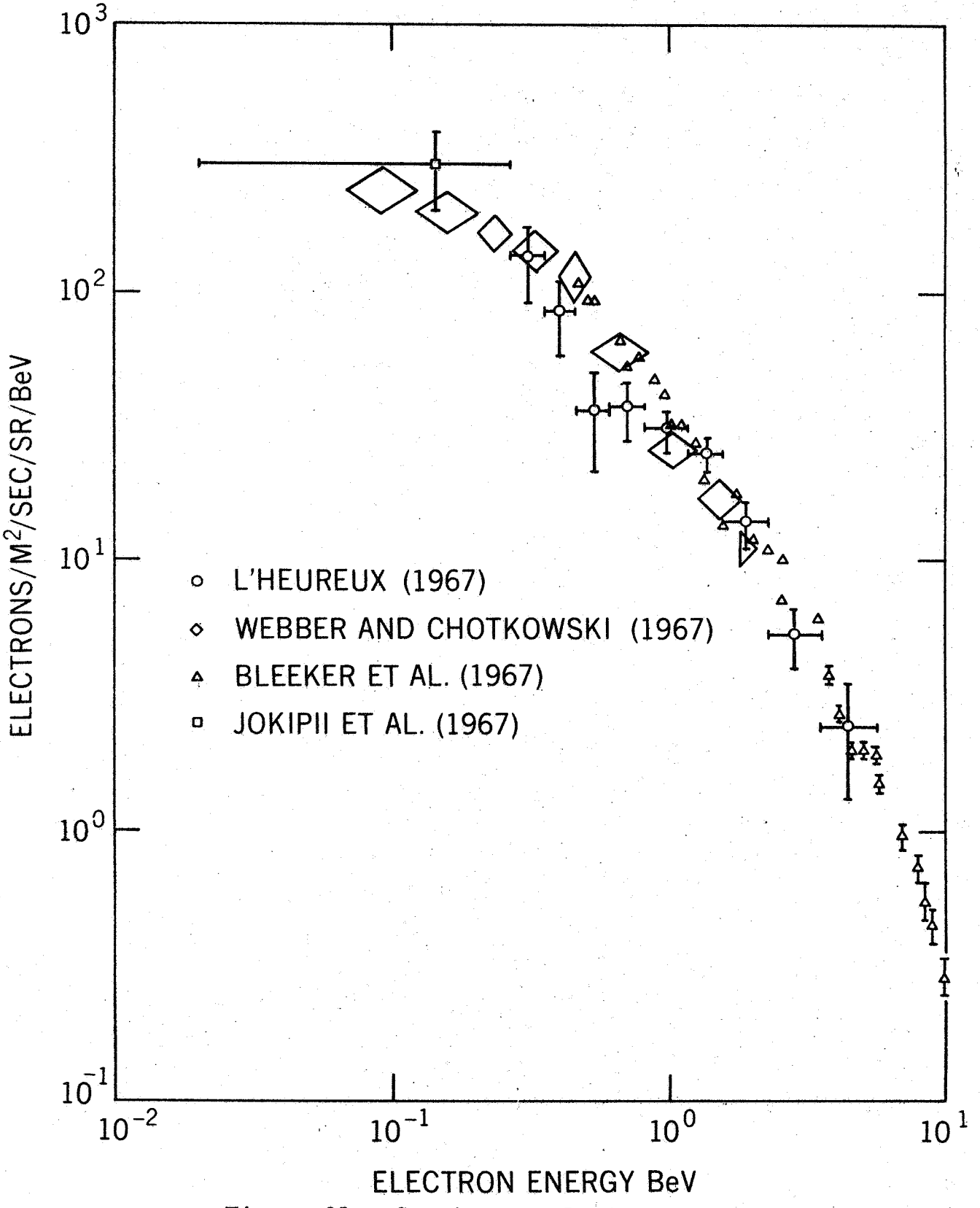

Figure 21. Cosmic ray electron spectrum.